A Numerical Study of Burgers' Equation With Robin Boundary Conditions

Vinh Q. Nguyen

Thesis submitted to the Faculty of the
Virginia Polytechnic Institute and State University
in partial fulfillment of the requirements for the degree of

Masters of Science
in
Mathematics

John Burns, Chair
Jeff Borggaard
Tao Lin

February 20, 2001
Blacksburg, Virginia

A Numerical Study of Burgers' Equation with Robin Boundary Conditions

Vinh Q. Nguyen

(ABSTRACT)

This thesis examines the numerical solution to Burgers' equation on a finite spatial domain with various boundary conditions. We first conduct experiments to confirm the numerical solutions observed by other researchers for Neumann boundary conditions. Then we consider the case where the non-homogeneous Robin boundary conditions approach the non-homogeneous Neumann conditions. Finally we numerically approximate the steady state solutions to Burgers' equation with both the homogeneous and non-homogeneous Robin boundary conditions.

Acknowledgments

I would like to express my deepest and grateful thanks to my advisor and committe chairman Dr. John Burns for his continuous encouragement, guidance, support, insight and patience with my work on this thesis. I would like to thank him for his general advice both on my academic endeavors and career goals. I would also like to thank him for his financial support during the past summer at Virginia Tech. I would also like to thank Dr. Jeff Borggard and Dr. Tao Lin for serving on my thesis committee and for their valuable guidance and encouragement on this thesis.

I would also like to give many thanks to my parents, my sisters and brothers for their love, support and encouragement. I thank them for having believed in me that I could achieve my goals and dreams. Without them, I would not have been here to pursue my educational endeavors.

I would like to thank all my friends that I have got to know here at Virginia Tech and in the Math Department. I would like to thank Chris Camphouse, Lynne Ryan and Michaela Schulze for their help and tips on using LaTeX and UNIX. I would also like to thank my office mates and great friends Hyung Oh, Lynne Ryan, Kenneth Massey, Michaela Schulze, Adrian Seaver, Marsha Wilson, Laurence Calzone, Dustin Potter and many many others for all the great times that we have had and have shared over the years at Virginia Tech.

Contents

List of Figures

List of Tables

Chapter 1

Introduction

1.1 A Brief History

For over sixty years, Burgers' equation has been studied and used as a simple model for many physically interesting problems and for convection-diffusion phenomena such as shock waves, turbulence, decaying free turbulence, traffic flows, flow-related problems, etc. The quasilinear parabolic equation

$$\frac{\partial u}{\partial t}(t,x) + u(t,x)\frac{\partial u}{\partial x}(t,x) = \epsilon\frac{\partial^2 u}{\partial x^2}(t,x) + f(t,x), \tag{1.1}$$

first appeared in a 1915 paper by Bateman [2], who used the equation as a model for the motion of a viscous fluid when the viscosity approaches zero, and derived two types of steady state solutions for the infinite domain problem. More than thirty years later, Johannes Martinus Burgers introduced the equation in his attempt to formulate a simple mathematical model that would show the fundamental features exhibited by the turbulence in hydrodynamic flows [3].

Following Burgers' initiative, there have been a lot of studies and research on the equation. Lighthill [9] formally derived the equation as second-order approximation to the one-dimensional unsteady Navier-Stokes equations. A similar result and observation was obtained by Moren and Shen [12] via the method of matched asymptotic expansion. Cole and

Hopf ([5], [7]) independently discovered that Burgers' equation with an initial condition on the infinite domain could be reduced to the linear heat equation by using a change in variables. A detailed discussion on this non-linear transformation will be discussed in a subsequent section of this chapter.

Burgers' equation is a quasi-linear parabolic partial differential equation that describes the time evolution of the function $u(t, x)$ under nonlinear convection and linear dissipation. When the viscosity ϵ is zero, the evolution of the function $u(t, x)$ may develop a shock. When ϵ is small, sharp gradients can develop and dissipate as $t \to \infty$.

The second ordered linear term $\epsilon \frac{\partial^2 u}{\partial x^2}$ in equation (1.1) is an elliptic differential operator. The problem, because of the non-linearity, exhibits many of features associated with singularity. This observation was illustrated by Fletcher in his paper published in 1982 [6]. He pointed out that Burgers' equation is a model equation for the balance between the nonlinear convective term and the diffusive term that may cause computational difficulties in for example fluid dynamic problems.

If we omit the convective term uu_x, the equation (1.1) becomes the classical heat equation. Dropping the diffusive term ϵu_{xx} from equation (1.1) yields the inviscous Burgers' equation, which is a hyperbolic equation that models the convection of disturbances in inviscous flow. Points on the solution to the inviscous Burgers' equation with larger u convect faster than points with smaller u, causing u to become discontinuous (i.e., a shock condition occurs) at a future time.

When the time derivative term of equation (1.1) is removed, we are left with the steady state equation of Burgers' equation, which is a non-linear elliptic equation that displays the balance between the convection and diffusion terms. A typical solution to the elliptic equation on the infinite spatial domain is sketched in Figure 1.1. The solution changes discontinuously as ϵ is approaching zero.

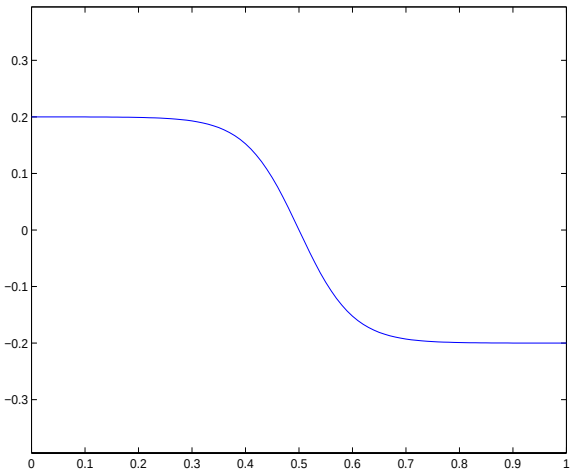

Figure 1.1: A typical solution of $uu_x = \epsilon u_{xx}$

1.2 Boundary conditions for Burgers' equation

Up to now, we have only discussed the general properties of Burgers' equation. We are now concerned with a finite spatial domain. For simplicity, we view Burgers' equation (1.1) as a perturbation to the linear heat equation, with the non-linear term uu_{xx} being the perturbation. We focus on the initial value problem

$$u_t(t,x) + u(t,x)u_x(t,x) = \epsilon u_{xx}(t,x) + f(t,x), \quad 0 < x < L, \quad t > 0 \tag{1.2}$$

$$u(0,x) = u_o(x), \quad 0 < x < L. \tag{1.3}$$

In order to have a well-posed partial differential equation problem, boundary conditions must be specified at the endpoints of the spatial domain. The first and probably the simplest type of boundary condition is the Dirichlet boundary condition, which specifies the solution value at the boundary

$$u(t,0) = g_1(t), \quad u(t,L) = g_2(t). \tag{1.4}$$

Since the equation (1.2) is of linear second order, it is also possible to specify the first derivative at the endpoints. Thus, one has the Neumann boundary condition

$$\kappa_1 u_x(t,0) = \kappa g_1(t), \quad \kappa_2 u_x(t,L) = \kappa g_2(t). \tag{1.5}$$

The third boundary condition is the linear combination of the Dirichlet and Neumann boundary conditions, called the Robin boundary condition

$$\kappa_1 u(t,0) - \kappa u_x(t,0) = \kappa_1 g_1(t), \qquad \kappa_2 u(t,L) + \kappa w_x(t,L) = \kappa_2 g_2(t). \tag{1.6}$$

Physically, a Dirichlet boundary condition usually corresponds to setting the value of a field variable. A Neumann boundary condition usually specifies a flux condition on the boundary. Notice that the Dirichlet and Neumann boundary conditions are special cases of the Robin boundary condition. Note in addition that mixed boundary conditions, say Dirichlet at the left endpoint and Neumann at the right, are physically possible as well.

It is often stated that the Cole-Hopf transformation transforms the problem (1.2) with the appropriate initial and boundary conditions to a linear boundary value problem. This, however, is only true in certain special cases as we shall see. We will apply the transformation for the initial value problem for Burgers' equation on the infinite domain. Then we will apply the transformation for the initial boundary value problems for Burgers' equation on a finite domain, say $0 < x < 1$.

1.3 The Cole-Hofp Transformation

The Cole-Hofp transformation often takes two stages. Consider the infinite domain problem

$$\begin{aligned} u_t + uu_x &= \epsilon u_{xx}, \quad -\infty < x < \infty \\ u(0,x) &= u_o(x). \end{aligned} \tag{1.7}$$

Introduce the function

$$u = \psi_x, \tag{1.8}$$

so that the equation (1.7) becomes

$$\psi_{xt} + \psi_x \psi_{xx} = \epsilon \psi_{xxx}, \tag{1.9}$$

and after integration with respect to x, the equation (1.9) becomes

$$\psi_t + \frac{1}{2}\psi_x^2 = \epsilon\psi_{xx}. \tag{1.10}$$

If

$$\psi = -2\epsilon \ln \phi, \tag{1.11}$$

then (1.10) yields

$$\frac{-2\epsilon}{\phi}\left(\phi_t - \epsilon\phi_{xx}\right) = 0, \tag{1.12}$$

which reduces to the diffusion equation

$$\phi_t = \epsilon\phi_{xx}. \tag{1.13}$$

Thus, the Cole-Hofp transformation $u = -2\epsilon\frac{\phi_x}{\phi}$, derived from (1.8) and (1.11), reduces Burgers' equation to the linear heat equation on $(-\infty, \infty)$. Applying the transformation to the initial condition for the problem (1.7), we have

$$u(0,x) = u_o(x) = -2\epsilon\frac{\phi_x(0,x)}{\phi(0,x)}. \tag{1.14}$$

Integrating both sides of (1.14) yields

$$\phi(0,x) = \phi_o(x) = \exp\left[-\frac{1}{2\epsilon}\int_0^x u_o(\xi)\,d\xi\right]. \tag{1.15}$$

It is known that the solution to the initial value problem ((1.13), (1.15)) on the infinite domain can be expressed as an integral form

$$\phi(t,x) = \frac{1}{\sqrt{(}4\pi\epsilon t)}\int_{-\infty}^{\infty}\phi_o(\xi)\exp\left[-\frac{(x-\xi)^2}{4\epsilon t}\right]\,d\xi. \tag{1.16}$$

Consequently, with the help of the Cole-Hofp transformation, we obtain the solution to the initial value problem for Burgers' equation on the infinite domain as follows

$$u(t,x) = \frac{\int_{-\infty}^{\infty}\left(\frac{x-\xi}{t}\right)\exp\left[-\frac{1}{2\epsilon}G(\xi,x,t)\right]\,d\xi}{\int_{-\infty}^{\infty}\exp\left[-\frac{1}{2\epsilon}G(\xi,x,t)\right]\,d\xi}, \tag{1.17}$$

where $G(\xi, x, t)$ is the integral function of the form

$$G(\xi, x, t) = \frac{(x-\xi)^2}{2t} + \int_0^{\xi} u_o(\tau)\, d\tau. \tag{1.18}$$

Consider (1.7) on a finite spatial domain, say $0 < x < 1$, together with the three boundary conditions discussed in the preceding section.

$$u_t + uu_x = \epsilon u_{xx}, \quad 0 < x < 1 \tag{1.19}$$
$$u(0, x) = u_o(x).$$

We begin with the nonhomogeneous Dirichlet boundary conditions

$$u(t, 0) = g_1(t), \qquad u(t, 1) = g_2(t).$$

Applying the Cole-Hofp transformation $u = -2\epsilon\frac{\phi_x}{\phi}$ to the boundary conditions, we get

$$\phi(t, 0)g_1(t) + 2\epsilon\phi_x(t, 0) = 0 \tag{1.20}$$
$$\phi(t, 1)g_2(t) + 2\epsilon\phi_x(t, 1) = 0. \tag{1.21}$$

In the homogeneous case, $g_1(t) = g_2(t) = 0$, the transformed boundary conditions are linear and of Neumann type. When $g_1(t) \neq 0$ and $g_2(t) \neq 0$, the transformed boundary conditions (1.20) - (1.21) are non-linear.

Consider the nonhomogeneous Neumann boundary conditions

$$u_x(t, 0) = g_1(t), \qquad u_x(t, 1) = g_2(t).$$

Again, we apply the transformation to the boundary conditions to get

$$(\phi(t, 0))^2 g_1(t) + 2\epsilon(\phi_{xx}(t, 0) - (\phi_x(t, 0))^2) = 0 \tag{1.22}$$
$$(\phi(t, 1))^2 g_2(t) + 2\epsilon(\phi_{xx}(t, 1) - (\phi_x(t, 1))^2) = 0. \tag{1.23}$$

Even if $g_1(t) = g_2(t) = 0$, the transformed boundary conditions have the second order spatial terms. Therefore the corresponding boundary value problem

$$\phi_t(t, x) = \epsilon\phi_{xx}(t, x)$$
$$\epsilon\phi_{xx}(t, 0) = 0$$
$$\epsilon\phi_{xx}(t, 1) = 0,$$

is not well posed.

For the nonhomogeneous Robin boundary conditions

$$u(t,0) - u_x(t,0) = g_1(t)$$
$$u(t,1) + u_x(t,1) = g_2(t),$$

the Cole-Hofp transformation yields

$$(\phi(t,0))^2 g_1(t) + 2\epsilon(\phi_x(t,0) - \phi_{xx}(t,0) + (\phi_x(t,0))^2) = 0 \tag{1.24}$$
$$(\phi(t,1))^2 g_2(t) + 2\epsilon(\phi_x(t,1) + \phi_{xx}(t,1) - (\phi_x(t,1))^2) = 0. \tag{1.25}$$

Again, we arrive at the same situation as in the Neumann case. Therefore, although the Cole-Hopf transformation nicely transforms the partial differential equation to a linear partial differential equation, the transformed boundary condition (Neumann or Robin) has non-linear terms. Thus the corresponding boundary value problem is not well-posed.

Another note that we would like to mention here is that if one considers the nonhomogeneous problem on the infinite spatial domain

$$u_t + uu_x = \epsilon u_{xx} + f(t,x), \quad -\infty < x < \infty \tag{1.26}$$
$$u(0,x) = u_o(x),$$

and then applies the Cole-Hofp transformation to this problem, one would not be able to get a non-homogeneous linear heat equation. In fact, after applying the transformation to (1.26), we obtain

$$\phi_t - \epsilon\phi_{xx} = -\frac{1}{2\epsilon}\hat{f}(t,x)\phi_x,$$

where $\hat{f}(t,x)$ is the anti-derivative of $f(t,x)$ with respect to x. However, no analytical solution is known to this problem when the form of $\hat{f}(t,x)$ is just any function of two variables.

1.4 Theoretical and Numerical Perspectives

As mentioned in the introduction, Burgers' equation has been used a model for many interesting physical phenomena and as a medium for testing and comparing numerical schemes. Therefore, it is not surprising to see that there have been many theories, numerical methods and observations developed for the equation.

G. Kreiss and H. Kreiss [8] considered the viscous Burgers' equation

$$u_t(t,x) + \frac{1}{2}[(u(t,x))^2]_x = \epsilon u_{xx}(t,x) + f(t,x), \quad t \geq 0, \quad 0 \leq x \leq 1, \qquad \epsilon > 0, \tag{1.27}$$

with the initial and non-homogeneous Dirichlet boundary conditions

$$u(x,0) = g(x), \qquad u(0,t) = a, \qquad u(1,t) = b.$$

The corresponding steady state to the above problem

$$\begin{aligned} \frac{1}{2}(y^2)_x &= \epsilon y_{xx} + f(x), \quad 0 \leq x \leq 1, \quad \epsilon > 0, \\ y(0) &= a, \quad y(1) = b. \end{aligned} \tag{1.28}$$

Solutions of (1.28) are called stationary or equilibrium solutions of the viscous equation (1.27). Kreiss and Kreiss were interested in the uniqueness, existence and properties of the steady steat equations (1.28). They attempted to develop numerical solutions for solving (1.28) by solving the time dependent problem (1.27) in hopes that for $t \to \infty$ the time dependent solution would converge to a unique steady state solution. They proved that if the equilibrium equation (1.28) has a solution, then it is unique; and that the equation (1.28) has a unique solution for all $\epsilon > 0$ [8]. Furthermore they noted, based on their numerical experiments, that the speed of convergence to the steady state solution depends on the location of the shock, and that if the shock is located in the interior, the speed of convergence is exponentially slow.

Motivated by the work done by Kreiss and Kreiss [8] in 1986, Reyna and Ward investigated

the shock layer behavior associated with the following problem [14]

$$\begin{aligned} u_t(t,x) + u(t,x)u_x(t,x) &= \epsilon u_{xx}(t,x), \quad 0 \le x \le 1, \quad t > 0, \\ u(0,t) &= \alpha > 0, \\ u(1,t) &= -\alpha, \\ u(x,0) &= \phi(x). \end{aligned} \tag{1.29}$$

One of Reyna's and Ward's main contributions was to give an analytical explanation for the exponentially slow phase where the shock layer drifts to its equilibrium point. Using the method of matched asymptotic expansion and knowing from symmetry that the equilibrium shock layer solution for the problem (1.29) is at $x = \frac{1}{2}$, they showed that there exists a one-parameter family of solutions to the corresponding steady state equation

$$v(x)v_x(x) - \epsilon v_{xx}(x) = 0 \tag{1.30}$$

given by

$$v(x) = -\alpha \ \tanh[\alpha\epsilon^{-1}(x - x_0)/2], \quad x_0 \in (0,1). \tag{1.31}$$

However, these functions only satisfy the boundary conditions to within exponentially small terms for any $x_0 \in (0,1)$ even though they do satisfy the equation (1.30). In an attempt to fix this problem, the authors in [14] examined the following problem

$$\begin{aligned} u_t(t,x) + u(t,x)u_x(t,x) &= \epsilon u_{xx}(t,x), \quad 0 \le x \le 1, \quad t > 0, \\ -\epsilon u_x(0,t) + K_l[u(0,t) - \alpha] &= 0, \quad \alpha > 0, \quad K_l > 0, \\ \epsilon u_x(1,t) + K_r[u(1,t) + \alpha] &= 0, \quad K_r > 0, \\ u(x,0) &= \phi(x), \end{aligned} \tag{1.32}$$

and the corresponding steady state problem

$$\begin{aligned} v(x)v_x(x) - \epsilon v_{xx}(x) &= 0, \\ -\epsilon v_x(0) + K_l[v(0) - \alpha] &= 0, \\ \epsilon v_x(1) + K_r[v(1) + \alpha] &= 0. \end{aligned}$$

The interesting feature of the problem (1.33) is that the existence and the stability of a shock condition depend on K_l and K_r as noted in [14]. For simplicity, the authors chose $K_l = K_r = K$ and arrived at a nontrivial equilibrium solution for the steady state problem

$$v(x) = -\beta \ \tanh[\beta\epsilon^{-1}(x - 1/2)/2] \tag{1.36}$$

where β is chosen to satisfy

$$-\frac{\beta^2}{2}\text{sech}^2\left(\frac{\beta\epsilon^{-1}}{4}\right) + K\left[\alpha - \beta \ \tanh\left(\frac{\beta\epsilon^{-1}}{4}\right)\right] = 0. \tag{1.37}$$

The authors specifically noted that for Burgers equation with $K_l = K_r = K$ there was an exchange of stability at $K = \alpha$. Furthermore, they showed that as $\epsilon \to \infty$ the principal eigenvalue of the linearization about the equilibrium solution to Burgers' equation satisfies

$$\alpha_0 \sim -2\alpha^2\left(1 - \frac{\alpha}{K}\right)e^{-\alpha\epsilon^{-1}/2} + \cdots . \tag{1.38}$$

When $\alpha < K$, the largest eigenvalue α_0 is negative and hence the solution given in (1.36) is linearly stable. Likewise α_0 is positive and the solution is linearly unstable, if $\alpha > K$.

It is interesting that numerically the problem (1.29) is related to the very recent work of Burns, Balogh, Gilliam, and Shubov in [4]. The authors considered Burgers' equation on the interval $(0, 1)$ with homogeneous Neuman boundary conditions

$$\begin{aligned} u_t(t,x) - \epsilon u_{xx}(t,x) + u(t,x)u_x(t,x) = 0, \qquad & t > 0, \\ u_x(0,t) = 0, & \\ u_x(1,t) = 0, & \\ u(x,0) = \phi(x). & \end{aligned} \tag{1.39}$$

It has been observed numerically that for small ϵ and *not too small* initial data, the numerical solution to the equation (1.39) converges to a non-constant function [13] as $t \to \infty$. Similar numerical results were also observed in [15]. Control problems using Neumann boundary condition for Burgers' equation also possess this numerical behavior [10]. It is recently known that these solutions are purely numerical, regardless of what numerical schemes are used to

solve the problem. Based on these observations, the authors conjectured the existence of some type of *Numerical Stationary Solutions* for the problem (1.39). They showed numerically that for the class of initial data consisting of *antisymmetric* functions (i.e. functions that are odd about $x = 1/2$ in the interval $(0, 1)$), this type of numerical anomaly would likely occur. For the problem (1.39), they gave a general form of non-constant solutions that is antisymmetric about $x = 1/2$ as below

$$h_B(x) = \sqrt{2c_0}\ \tanh\left(\frac{\sqrt{2c_0}}{2\epsilon}(1/2 - x)\right) \tag{1.40}$$

They showed that for suitable initial data and c_0, the functions in (1.40) are actually numerical stationary solutions to problem (1.39). That is, they satisfy the Burgers' equation and they approximately satisfy the boundary conditions to within the exponentially small terms. Namely, the function in (1.40) satisfies equation (1.39) exactly.

1.5 Goals

Motivated by the recent works in([1], [4], [14]), we would like to numerically examine the Burgers' equation with the Robin boundary conditions. We consider the problem

$$\begin{aligned}
\frac{\partial w}{\partial t}(t,x) + w(t,x)\frac{\partial w}{\partial x}(t,x) &= \epsilon\frac{\partial^2 w}{\partial x^2}(t,x), \qquad 0 < x < L, \qquad t > 0, \\
\kappa_1 w(t,0) - \kappa\frac{\partial w}{\partial x}(t,0) &= \alpha_1, \\
\kappa_2 w(t,L) + \kappa\frac{\partial w}{\partial x}(t,L) &= \alpha_2, \\
w(0,x) &= w_o(x).
\end{aligned} \tag{1.41}$$

Both of α_1 and α_2 are to be computed by the following

$$\alpha_1 = \kappa_1 h(0) - \kappa h'(0), \tag{1.42}$$

$$\alpha_2 = \kappa_2 h(L) + \kappa h'(L), \tag{1.43}$$

where the function $h(x)$ is antisymmetric at $x = L/2$ on the interval $(0, L)$

$$h(x) = \sqrt{2c_0}\ \tanh\left(\frac{\sqrt{2c_0}}{2\epsilon}(L/2 - x)\right). \tag{1.44}$$

Here ϵ and κ can be related by $\epsilon = \frac{\kappa}{\rho c}$, where ρ is the density of the material and c the specific heat. The constants κ, κ_1 and κ_2 are the thermal conductivities of the materials.

A standard Finite Element scheme will be used to approximate this problem. The Finite Element scheme will be discussed in Chapter 2. The numerical examples and experiments will be presented in Chapter 3. An explanation for the existence of the tanh function in the problem will also be discussed in Chapter 3. Conclusion and Open Problems will conclude this paper.

Chapter 2

Finite Element Methods

2.1 Bugers' Equation Revisited

We consider the initial-boundary value problem (IBVP)

$$\frac{\partial w}{\partial t}(t,x) + w(t,x)\frac{\partial w}{\partial x}(t,x) = \epsilon\frac{\partial^2 w}{\partial x^2}(t,x) + f(t,x), \quad 0 < x < L, \quad t > 0, \tag{2.1}$$

with the Robin's boundary conditions

$$\frac{\kappa_1}{L_1}w(t,0) - \kappa\frac{\partial w}{\partial x}(t,0) = \frac{\kappa_1}{L_1}u_1(t), \qquad \frac{\kappa_2}{L_2}w(t,L) + \kappa\frac{\partial w}{\partial x}(t,L) = \frac{\kappa_2}{L_2}u_2(t) \tag{2.2}$$

and the initial condition

$$w(0,x) = w_o(x). \tag{2.3}$$

It may be helpful to think of $w(t,x)$ as heat flow through a metal rod at time t and position x as described in Smith [15]. The constant κ is the thermal conductivity of the rod, ϵ the thermal diffusitivity. They are related by the formula $\epsilon = \frac{\kappa}{\rho c}$, where ρ is the density of the material, and c its specific heat. The constants κ_1 and κ_2 are the thermal conductivities of the thin film coated at both ends of the rod of length L_1 and L_2, respectively.

2.2 The Weak Form Problem

Let $\Omega = (0, L)$ be the spatial domain, and let $v(\cdot) \in H^1(\Omega)$ be a test function, where $H^1(\Omega)$ is the Sobolev space

$$H^1(\Omega) = \Big\{ v \Big| v \in L_2(\Omega), v_x \in L_2(\Omega) \Big\}. \tag{2.4}$$

Multiply both sides of the equation (2.1) by $v(\cdot)$ and integrate, we get

$$\int_0^L \frac{\partial w}{\partial t}(t,x)v(x)\,dx + \int_0^L w(t,x)\frac{\partial w}{\partial x}(t,x)v(x)\,dx = \int_0^L \epsilon \frac{\partial^2 w}{\partial x^2}(t,x)v(x)\,dx + \int_0^L f(t,x)v(x)\,dx. \tag{2.5}$$

Bring the second term on the left hand side to the right and then integrate by parts, we obtain

$$\int_0^L \frac{\partial w}{\partial t}(t,x)v(x)\,dx = -\int_0^L w(t,x)\frac{\partial w}{\partial x}(t,x)v(x)\,dx - \int_0^L \epsilon \frac{\partial w}{\partial x}(t,x)v'(x)\,dx + \epsilon\left[\frac{\partial w}{\partial x}(t,x)v(x)\right]_0^L + \int_0^L f(t,x)v(x)\,dx. \tag{2.6}$$

A simple straight forward substitution yields the weak form for the problem

$$\int_0^L \frac{\partial w}{\partial t}(t,x)v(x)\,dx = -\int_0^L w(t,x)\frac{\partial w}{\partial x}(t,x)v(x)\,dx - \int_0^L \epsilon \frac{\partial w}{\partial x}(t,x)v'(x)\,dx + \epsilon\frac{\partial w}{\partial x}(t,L)v(L) - \epsilon\frac{\partial w}{\partial x}(t,0)v(0) + \int_0^L f(t,x)v(x)\,dx. \tag{2.7}$$

Typically, when using finite elment methods to solve an initial boundary value problem, one often obtains the weak formulation for the problem before selecting the test function space based on the weak form equation and on the boundary conditions. In problem (2.1), we are dealing with the non-homogeneous Robin boundary conditions and therefore, $H^1(\Omega)$ should be the test function space. However if, for example the homogeneous Dirichlet boundary conditions are the case, then $H_0^1(\Omega)$ should be considered. The difference between H^1 and H_0^1 is that the later consists of functions that vanish on the boundary of the domain. In this case, the third and fourth terms of the weak form equation (2.7) will vanish at $\partial\Omega$, the boundary of Ω.

2.3 Piecewise Linear Basis Functions and Finite Element Spaces

We denote V_h as the function space consisting of piecewise linear polynomials. Clearly, V_h is a subspace of H^1. For simplicity, we assume that $L = 1$, and for convenient the discretization parameter h is taken to be $h = \frac{1}{N+1}$. We then divide the interval $[0, 1]$ into N+1 equal subintervals $[x_i, x_{i+1}]$, $x_i = \frac{i}{N+1}$, $i = 0, 1, 2, \cdots, N+1$. For each i, we let $h_i(x)$ denote the linear spline basis function defined by

$$h_0(x) = \begin{cases} -(N+1)(x - x_1), & x_0 \le x \le x_1 \\ 0, & otherwise \end{cases}$$

$$h_i(x) = \begin{cases} (N+1)(x - x_{i-1}), & x_{i-1} \le x \le x_i \\ -(N+1)(x - x_{i+1}), & x_i \le x \le x_{i+1} \\ 0, & otherwise \end{cases}$$

for $1 \le i \le N$, and

$$h_{N+1}(x) = \begin{cases} (N+1)(x - x_N), & x_N \le x \le x_{N+1} \\ 0, & otherwise. \end{cases}$$

Let $V_h \equiv V_h^N \subset H^1(0, L)$ be the $(N+1)$ dimensional finite element space given by

$$V_h^N = \left\{ \sum_{i=0}^{N+1} \alpha_i h_i(x) : \alpha_i \in \Re, i = 0, 1, \cdots, N+1 \right\}.$$

The approximate solution $w^N(t, x)$ to the exact solution $w(t, x)$ for the IBVP is given by

$$w^N(t, x) = \sum_{i=0}^{N+1} \alpha_i(t) h_i(x), \tag{2.8}$$

where each coefficient $\alpha_i(\cdot)$ is a nodal unknown, and $h_i(\cdot)$ is the i^{th} linear basis function defined on [0,1]. These approximations $w^N(t, x)$ will be used to generate an N+2 dimensional time-dependent system of ordinary differential equations in the weak formulation of the Galerkin and the Conservation Galerkin methods.

2.4 The Galerkin Approximation

In this section, we will derive the weak formulation of the Galerkin approximation for the Burgers' equation with the non-homogeneous Robin boundary conditions. Substitute the approximate solution $w^N(t,x)$ into the weak form (2.6), we get the first order non-linear differential equation for the vector function

$$\begin{aligned}\int_0^L \left[\sum_{i=0}^{N+1} \dot{\alpha}_i(t)h_i(x)\right] h_j(x)\,dx = &-\int_0^L \left[\sum_{i=0}^{N+1} \alpha_i(t)h_i(x)\sum_{k=0}^{N+1} \alpha_k(t)h_k'(x)\right] h_j(x)\,dx \\ &- \epsilon\int_0^L \sum_{i=0}^{N+1} \alpha_i(t)h_i'(x))h_j'(x)\,dx \\ &+ \epsilon\left[\sum_{i=0}^{N+1} \alpha_i(t)h_i'(x)h_j(x)\right]_0^L + \int_0^L f(t,x)h_j(x)\,dx \qquad (2.9)\end{aligned}$$

for $0 \le j \le N+1$. Substituting in the boundary conditions and rearranging all terms yield

$$\begin{aligned}\sum_{i=0}^{N+1}\left[\int_0^L h_i(x)hj(x)dx\right]\dot{\alpha}_i(t) = &-\sum_{i=0}^{N+1}\sum_{k=0}^{N+1}\left[\int_0^L h_i(x)h_k'(x)h_j(x)\,dx\right]\alpha_i(t)\alpha_k(t) \\ &- \epsilon\sum_{i=0}^{N+1}\left[\int_0^L h_i'(x)h_j'(x)\,dx\right]\alpha_i(t) - \epsilon\frac{\kappa_1}{\kappa L_1}\alpha_0(t)h_j(0) \\ &- \epsilon\frac{\kappa_2}{\kappa L_2}\alpha_{N+1}(t)h_j(L) + \epsilon\frac{\kappa_1}{\kappa L_1}u_1(t)h_j(0) \\ &+ \epsilon\frac{\kappa_2}{\kappa L_2}u_2(t)h_j(L) + \int_0^L f(t,x)h_j(x)\,dx, \qquad 0 \le j \le N+1. \qquad (2.10)\end{aligned}$$

Observe that the only term on the left of equation (2.10) can be written as $[M^N]\vec{\dot{\alpha}}(t)$ where

$$\vec{\dot{\alpha}}(t) = \begin{bmatrix} \dot{\alpha}_0(t) \\ \dot{\alpha}_1(t) \\ \vdots \\ \dot{\alpha}_{N+1}(t) \end{bmatrix},$$

and the matrix $[M^N]$, known as the global mass matrix, has entries given by

$$m_{ij} = \int_0^L h_i(x)h_j(x)\,dx, \qquad 1 \le i,j \le N+1,$$

is the (N+2)x(N+2) tridiagonal matrix

$$\left[M^N\right] = \frac{L}{6(N+1)} \begin{bmatrix} 2 & 1 & 0 & 0 & & \dots & 0 \\ 1 & 4 & 1 & 0 & & \dots & 0 \\ 0 & 1 & 4 & 1 & 0 & \dots & 0 \\ & & \ddots & \ddots & \ddots & & \vdots \\ \vdots & & & \ddots & \ddots & \ddots & \\ 0 & \dots & & 0 & 1 & 4 & 1 \\ 0 & \dots & & & 0 & 1 & 2 \end{bmatrix}_{(N+2)X(N+2)} .$$

The first term on the right of equation (2.10) gives the non-linear vector functional of $\vec{\alpha}(t)$ that approximates the non-linear term $w(t,x)w_x(t,x)$ of the Burgers' equation. Because of the non-linearity, this vector functional, denoted as $J(\vec{\alpha}(t))$, would complicate the approximate solution for the Burgers' equation when N is large.

$$J(\vec{\alpha}(t)) = \frac{1}{6} \begin{bmatrix} -2[\alpha_0(t)]^2 + \alpha_0(t)\alpha_1(t) + [\alpha_1(t)]^2 \\ -[\alpha_0(t)]^2 - \alpha_0(t)\alpha_1(t) + \alpha_1(t)\alpha_2(t) + [\alpha_2(t)]^2 \\ \vdots \\ -[\alpha_{N-1}(t)]^2 - \alpha_{N-1}(t)\alpha_N(t) + \alpha_N(t)\alpha_{N+1}(t) + [\alpha_{N+1}(t)]^2 \\ -[\alpha_N(t)]^2 + \alpha_N(t)\alpha_{N+1}(t) + 2[\alpha_{N+1}(t)]^2 \end{bmatrix}_{(N+2)X1} .$$

The second term on the right of equation (2.10) can also be written as $[S^N]\vec{\alpha}(t)$, where

$$\vec{\alpha}(t) = \begin{bmatrix} \alpha_0(t) \\ \alpha_1(t) \\ \vdots \\ \alpha_{N+1}(t) \end{bmatrix}_{(N+2)X1} ,$$

and the matrix $\left[S^N\right]$, known as the global stiffness matrix, has entries given by

$$s_{ij} = \int_0^L h_i'(x)h_j'(x)\,dx, \qquad 1 \le i,j \le N+1.$$

However, before computing the entries s_{ij} for the stiffness matrix, we notice that the third and the fourth terms on the right hand side of equation (2.10) also involve elements of

the unknown vector $\vec{\alpha}(t)$, namely $\alpha_0(t)$ and $\alpha_{N+1}(t)$, which add to the (1,1) and (N+2,N+2) entries of the global matrix $\left[S^N\right]$. Hence we get the adjusted global stiffness matrix, denoted as $\left[K^N\right]$ as follows

$$\left[K^N\right] = \frac{(N+1)}{L}\begin{bmatrix} -1-\dfrac{\kappa_1 L}{(N+1)\kappa L_1} & 1 & 0 & & \dots & 0 \\ 1 & -2 & 1 & 0 & \dots & 0 \\ 0 & 1 & -2 & 1 & 0 \dots & 0 \\ & & \ddots & \ddots & \ddots & \vdots \\ \vdots & & & \ddots & \ddots & 0 \\ 0 & & \dots & 0 & 1 & -2 & 1 \\ 0 & & \dots & & 0 & 1 & -1-\dfrac{\kappa_2 L}{(N+1)\kappa L_2} \end{bmatrix}_{(N+2)X(N+2)}.$$

Observe that the fifth and the sixth terms on the right hand side of equation (2.10) form an (N+2)x2 matrix. If we let $\vec{u}(t) = [u_1(t) \quad u_2(t)]^T$ be the so-called control vector, then we can see that the remaining matrix, denoted as $\left[G^N\right]$, becomes

$$\left[G^N\right] = \begin{bmatrix} \dfrac{\kappa_1}{\kappa L_1} & 0 \\ 0 & 0 \\ \vdots & \vdots \\ 0 & 0 \\ 0 & \dfrac{\kappa_2}{\kappa L_2} \end{bmatrix}_{(N+2)X2}.$$

And finally, the forcing term on the right of equation (2.10) yields the vector function

$$F^N(t) = \begin{bmatrix} \int_0^L f(t,x)h_0(x)\,dx \\ \int_0^L f(t,x)h_1(x)\,dx \\ \vdots \\ \vdots \\ \int_0^L f(t,x)h_{N+1}(x)\,dx \end{bmatrix}_{(N+2)X1}.$$

The equation (2.10) can now be written as a system of N+2 dimensional ordinary differential equations

$$\Big[M^N\Big]\dot{\vec{\alpha}}(t) = -J(\vec{\alpha}(t)) + \epsilon\Big[K^N\Big]\vec{\alpha}(t) + \epsilon\Big[G^N\Big]\vec{u}(t) + F^N(t). \tag{2.11}$$

Since the matrix mass is positive definite, it is invertible and so we get the differential equation for (2.10)

$$\dot{\vec{\alpha}}(t) = -\Big[M^N\Big]^{-1}J(\vec{\alpha}(t)) + \epsilon\Big[M^N\Big]^{-1}\Big[K^N\Big]\vec{\alpha}(t) + \epsilon\Big[M^N\Big]^{-1}\Big[G^N\Big]\vec{u}(t) + \Big[M^N\Big]^{-1}F^N(t), \tag{2.12}$$

or equivalently

$$\dot{\vec{\alpha}}(t) = -\Big[M^N\Big]^{-1}J(\vec{\alpha}(t)) + \epsilon\Big[A^N\Big]\vec{\alpha}(t) + \epsilon\Big[B^N\Big]\vec{u}(t) + \widehat{F}^N(t). \tag{2.13}$$

Having obtained the differential equation for (2.10), we turn our focus on how to obtain the initial condition. Multiplying both sides of (2.3) by $v(x)$, integrating over the interval [0,L], and then expanding it in the linear basis functions, we get

$$\int_0^L \sum_{i=0}^{N+1} \alpha_i(0)h_i(x)h_j(x)\,dx = \int_0^L w_o(x)h_j(x)\,dx, \tag{2.14}$$

for $j = 0, 1, 2, ..., N+1$. By inspection, we see that the left term can be written as $\Big[M^N\Big]\vec{\alpha}_o$, where $\Big[M^N\Big]$ is again the global mass matrix and $\vec{\alpha}_o$ is the vector

$$\vec{\alpha}(0) = \begin{bmatrix} \alpha_0(0) \\ \alpha_1(0) \\ \vdots \\ \vdots \\ \alpha_{N+1}(0), \end{bmatrix}_{(N+2)X1}.$$

The right side of equation (2.14) is the (N+2)-dimensional vector

$$w_o^N = \begin{bmatrix} \int_0^L w_o(x)h_0(x)\,dx \\ \int_0^L w_o(x)h_1(x)\,dx \\ \vdots \\ \vdots \\ \int_0^L w_o(x)h_{N+1}(x)\,dx \end{bmatrix}_{(N+2)X1}.$$

Hence for the intial condition, we have $\left[M^N\right]\vec{\alpha}_o = w_o^N$. Then multiply both sides by $\left[M^N\right]^{-1}$ to obtain the final form of the initial condition: $\vec{\alpha_o} = \left[M^N\right]^{-1} w_o^N$. Thus, we want to solve the differential equation

$$\dot{\vec{\alpha}}(t) = -\left[M^N\right]^{-1} J(\vec{\alpha}(t)) + \epsilon\left[A^N\right]\vec{\alpha}(t) + \epsilon\left[B^N\right]\vec{u}(t) + \widehat{F}^N(t) \tag{2.15}$$

with the initial condition

$$\vec{\alpha}_o = \left[M^N\right]^{-1} w_o^N.$$

2.5 The Galerkin/Conservation Method

Recall that the non-linear term of Burgers' equation is $w(t,x)w_x(t,x)$. Note that it can be written as $\frac{1}{2}(w^2)_x$. Hence we have the alternate form of the equation (2.1) as follows

$$\frac{\partial w}{\partial t}(t,x) + \frac{1}{2}\frac{\partial w^2}{\partial x}(t,x) = \epsilon\frac{\partial^2 w}{\partial x^2}(t,x) + f(t,x). \tag{2.16}$$

As before, we will derive the weak form for the problem. Multiply both sides of equation (2.16) by a test function $v(\cdot)$ and integrate, we get

$$\begin{aligned}\int_0^L \frac{\partial w}{\partial t}(t,x)v(x)\,dx + \int_0^L \frac{1}{2}\frac{\partial w^2}{\partial x}(t,x)v(x)\,dx = \int_0^L \epsilon\frac{\partial^2 w}{\partial x^2}(t,x)v(x)\,dx \\ + \int_0^L f(t,x)v(x)\,dx.\end{aligned} \tag{2.17}$$

Integrate the second order term by parts and rearrange terms to get the weak form

$$\begin{aligned}\int_0^L \frac{\partial w}{\partial t}(t,x)v(x)\,dx = -\int_0^L \frac{1}{2}\frac{\partial}{\partial x}[w^2(t,x)]v(x)\,dx - \epsilon\int_0^L \frac{\partial w}{\partial x}(t,x)v'(x)\,dx \\ + \epsilon\frac{\partial w}{\partial x}(t,L)v(L) - \epsilon\frac{\partial w}{\partial x}(t,0)v(0) + \epsilon\int_0^L f(t,x)v(x)\,dx.\end{aligned} \tag{2.18}$$

Again choose $v(x) = h_i(x)$, the linear basis functions decribed previously as the test functions. Since there is a quadratic term of $w(t,x)$ in the weak form, we need to postulate the

approximate solution $(w^N(t,x))^2$ to $w^2(t,x)$ as below

$$[w^N(t,x)]^2 = \sum_{i=0}^{N+1} (\alpha_i(t))^2 h_i(x). \tag{2.19}$$

Substitute $h_i(x)$, $[w^N(t,x)]^2$, and $w^N(t,x)$ into the weak form of the equation, and substitute in the boundary conditions to get the following semi-discritized equation

$$\begin{aligned}\int_0^L \left[\sum_{i=0}^{N+1} \dot{\alpha}_i(t) h_i(x)\right] h_j(x)\,dx = &-\frac{1}{2}\int_0^L \left[\sum_{i=0}^{N+1} (\alpha_i(t))^2 h_i'(x)\right] h_j(x)\,dx \\ &- \epsilon \int_0^L \sum_{i=0}^{N+1} \alpha_i(t) h_i'(x)) h_j'(x)\,dx \\ &+ \epsilon \left(\sum_{i}^{N+1} \alpha_i(t) h_i'(L) h_j(L)\right) - \epsilon \left(\sum_{i}^{N+1} \alpha_i(t) h_i'(0) h_j(0)\right) \\ &+ \int_0^L f(t,x) h_j(x)\,dx, \qquad 0 \le j \le N+1. \end{aligned} \tag{2.20}$$

Rearranging terms yields

$$\begin{aligned}\sum_{i=0}^{N+1} \left[\int_0^L h_i(x) hj(x) dx\right] \dot{\alpha}_i(t) = &-\frac{1}{2}\sum_{i=0}^{N+1} \left[\int_0^L h_i'(x) h_j(x)\,dx\right] (\alpha_i(t))^2 \\ &- \epsilon \sum_{i=0}^{N+1} \left[\int_0^L h_i'(x) h_j'(x)\,dx\right] \alpha_i(t) - \epsilon \frac{\kappa_1}{\kappa L_1} \alpha_0(t) h_j(0) - \epsilon \frac{\kappa_2}{\kappa L_2} \alpha_{N+1}(t) h_j(L) \\ &+ \epsilon \frac{\kappa_1}{\kappa L_1} u_1(t) h_j(0) + \epsilon \frac{\kappa_2}{\kappa L_2} u_2(t) h_j(L) \\ &+ \int_0^L f(t,x) h_j(x)\,dx, \qquad 0 \le j \le N+1. \end{aligned} \tag{2.21}$$

This reduces to the system of differential equations

$$\left[M^N\right] \begin{bmatrix} \dot{\alpha}_0(t) \\ \dot{\alpha}_1(t) \\ \vdots \\ \dot{\alpha}_{N+1}(t) \end{bmatrix} = \left[D^N\right] \begin{bmatrix} (\alpha_0(t))^2 \\ (\alpha_1(t))^2 \\ \vdots \\ (\alpha_{N+1}(t))^2 \end{bmatrix} + \epsilon \left[K^N\right] \begin{bmatrix} \alpha_0(t) \\ \alpha_1(t) \\ \vdots \\ \alpha_{N+1}(t) \end{bmatrix} + \epsilon \left[G^N\right] \begin{bmatrix} u_1(t) \\ u_2(t) \end{bmatrix} + F^N(t), \tag{2.22}$$

where $\left[M^N\right]$, $\left[K^N\right]$, $\left[G^N\right]$, and $F^N(t)$ are the same as in section 2.4. The matrix $\left[D^N\right]$ with given by $d_{ij} = \frac{1}{2}\int_0^L hi'(x)h'_j(x)\,dx$ has the form

$$\left[D^N\right] = \frac{1}{4}\begin{bmatrix} -1 & 1 & 0 & 0 & & \dots & 0 \\ -1 & 0 & 1 & 0 & & \dots & 0 \\ 0 & -1 & 0 & 1 & 0 & \dots & 0 \\ & & \ddots & \ddots & \ddots & & \vdots \\ \vdots & & & \ddots & \ddots & \ddots & \vdots \\ 0 & \dots & & 0 & -1 & 0 & 1 \\ 0 & \dots & & & 0 & -1 & 1 \end{bmatrix}_{(N+2)X(N+2)}.$$

Finally, we obtain the system of N+2 dimensional ordinary differential equations

$$\left[M^N\right]\ddot{\vec{\alpha}}(t) = -J_C(\vec{\alpha}(t)) + \epsilon\left[K^N\right]\vec{\alpha}(t) + \epsilon\left[G^N\right]\vec{u}(t) + F^N(t), \tag{2.23}$$

where $J_C(\vec{\alpha}(t))$ represents the non-linear vector functional of $\vec{\alpha}(t)$ that approximates the non-linear term $(w_x(t,x))^2$ of the alternative form of Burgers' equation

$$J_c(\vec{\alpha}(t)) = \frac{1}{4}\begin{bmatrix} (\alpha_1(t))^2 - (\alpha_0(t))^2 \\ (\alpha_2(t))^2 - (\alpha_0(t))^2 \\ (\alpha_3(t))^2 - (\alpha_1(t))^2 \\ \vdots \\ (\alpha_N(t))^2 - (\alpha_{N-2}(t))^2 \\ (\alpha_{N+1}(t))^2 - (\alpha_{N-1}(t))^2 \\ (\alpha_{N+1}(t))^2 - (\alpha_N(t))^2 \end{bmatrix}_{(N+2)X1}.$$

As before, since $\left[M^N\right]$ is invertible so the preceding equation may be multiplied by $\left[M^N\right]^{-1}$ to finally obtain the system

$$\ddot{\vec{\alpha}}(t) = -\left[M^N\right]^{-1} J_C(\vec{\alpha}(t)) + \epsilon\left[A^N\right]\vec{\alpha}(t) + \epsilon\left[B^N\right]\vec{u}(t) + \widehat{F}^N(t), \tag{2.24}$$

where $\left[A^N\right]$, $\left[B^N\right]$, and $\widehat{F}^N(t)$ are defined as before. The initial condtion $\vec{\alpha_0}$ for this problem is exactly the same like the one described near the end of Section 2.4.

As far as convergence is concerned, the Conservation/Galerkin Method seems to converge faster than the Galerkin Method (See [13], [15], and [11]). We will apply the Conservation/Galerkin Method to problem (1.41), which we restate here again

$$\begin{aligned} \frac{\partial w}{\partial t}(t,x) + w(t,x)\frac{\partial w}{\partial x}(t,x) &= \epsilon \frac{\partial^2 w}{\partial x^2}(t,x), \qquad 0 < x < L, \qquad t > 0, \qquad (2.25)\\ \kappa_1 w(t,0) - \kappa \frac{\partial w}{\partial x}(t,0) &= \alpha_1,\\ \kappa_2 w(t,L) + \kappa \frac{\partial w}{\partial x}(t,L) &= \alpha_2,\\ w(0,x) &= w_o(x). \end{aligned}$$

Both of α_1 and α_2 are to be computed by the following

$$\alpha_1 = \kappa_1 h(0) - \kappa h'(0), \qquad (2.26)$$

$$\alpha_2 = \kappa_2 h(L) + \kappa h'(L), \qquad (2.27)$$

where the function $h(x)$ is anti-symmetric at $x = L/2$ on the interval $(0, L)$

$$h(x) = \sqrt{2c_0}\ \tanh\left(\frac{\sqrt{2c_0}}{2\epsilon}(L/2 - x)\right). \qquad (2.28)$$

The mass matrix $\left[M^N\right]$ and the stiffness matrix $\left[K^N\right]$ are the same as discussed earlier, except for the fact that now the terms L_1 and L_2 appearing in these matrices are being set to 1. Since the problem we are interested in is homogeneous, we would not have the forcing term F^N in the system of differential equations. However, the two non-zero entries of the $(N+2)X2$ matrix $\left[G^N\right]$ are being changed, and thus $\left[G^N\right]$ now takes the form

$$\left[G^N\right] = \begin{bmatrix} \frac{\alpha_1}{\kappa} & 0 \\ 0 & 0 \\ \vdots & \vdots \\ 0 & 0 \\ 0 & \frac{\alpha_2}{\kappa} \end{bmatrix}.$$

We will use MATLAB to develop finite element code for the problem. We will also use the differential equation solver ODE23S for solving the system of differential equations that we have discussed in this chapter.

Chapter 3

Numerical Experiments

In this chapter, we will approximate the solutions to Burgers' equation on a finite domain with various boundary conditions. We start the numerical experiments by an example with known solution. Then we numerically solve Burgers' equation on the finite domain with the Neumann (homogeneous and non-homogeneous) boundary conditions to confirm the numerical solutions observed by other researchers. We continue the numerical experiments by considering the problem where the non-homogeneous Robin condition approaches the non-homogeneous Neumann condition. Finally, we conduct numerical experiments for the problem with Robin (non-homogeneous and homogeneous) boundary conditions.

3.1 A Starting Example

Consider the Burgers' equation

$$\frac{\partial w}{\partial t}(t,x) + w(t,x)\frac{\partial w}{\partial x}(t,x) = \epsilon \frac{\partial^2 w}{\partial x^2}(t,x) + f(t,x),$$

with the nonhomogeneous Robin's boundary conditions

$$\frac{\kappa_1}{L_1}w(t,0) - \kappa\frac{\partial w}{\partial x}(t,0) = \frac{\kappa_1}{L_1}u_1(t); \qquad \frac{\kappa_2}{L_2}w(t,L) + \kappa\frac{\partial w}{\partial x}(t,L) = \frac{\kappa_2}{L_2}u_2(t),$$

and the initial condition

$$w(0,x) = w_o(x).$$

Assume that the explicit form of a solution $w(t,x)$ is given. From the Burgers' equation and the boundary conditions, we solve for $f(t,x)$, $u_1(t)$ and $u_2(t)$ to get

$$\begin{aligned} f(t,x) &= w_t(t,x) + w(t,x)w_x(t,x) - \epsilon w_{xx}(t,x), \\ u_1(t) &= w(t,0) - \frac{\kappa L_1}{\kappa_1} w_x(t,0), \\ u_2(t) &= w(t,L) + \frac{\kappa L_2}{\kappa_2} w_x(t,L). \end{aligned}$$

We are now ready to present an example with a known solution. This example can also be found in [15].

Example 3.1 Choose $L = 100, L_1 = L_2 = 10, \kappa = .93, \kappa_1 = \kappa_2 = .55$, and $\epsilon = 1.14$ (See Table 1.2.1 in [15]) and suppose that $w(t,x)$ is given as

$$w(t,x) = \frac{(100-x)^2}{10^4} sin(\alpha t) + \frac{x^2}{10^4} cos(\beta t).$$

By the above formulas, we obtain the forcing term

$$\begin{aligned} f(t,x) = \alpha \frac{(100-x)^2}{10^4} cos(\alpha t) - \beta \frac{x^2}{10^4} sin(\beta t) - 2\frac{(100-x)^3}{10^8} sin^2(\alpha t) + 2\frac{x^3}{10^8} cos^2(\beta t) \\ + \frac{2}{10^8}(2x^3 - 300x^2 + 10^4 x) sin(\alpha t) cos(\beta t) - \frac{2\epsilon}{10^4}(sin(\alpha t) + cos(\beta t)), \end{aligned}$$

and the boundary functions and the initial condition

$$\begin{aligned} u_1(t) &= \left(1 + \frac{2\kappa L_1}{100\kappa_1}\right) sin(\alpha t), \\ u_2(t) &= \left(1 + \frac{2\kappa L_2}{100\kappa_2}\right) cos(\beta t), \\ w_o(x) &= w(0,x) = \frac{x^2}{10^4}. \end{aligned}$$

Choose α and β to be 1.5π and $.5\pi$ respectively. The exact solution is shown on Figure 3.1, and the numerical solution generated by the Conservation/Galerkin method for N = 16 is

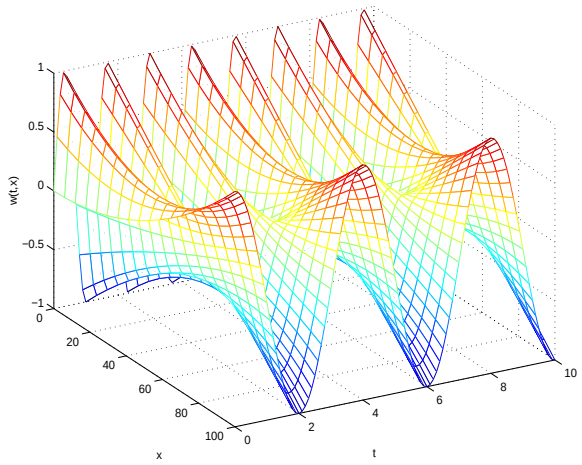

Figure 3.1: Exact solution

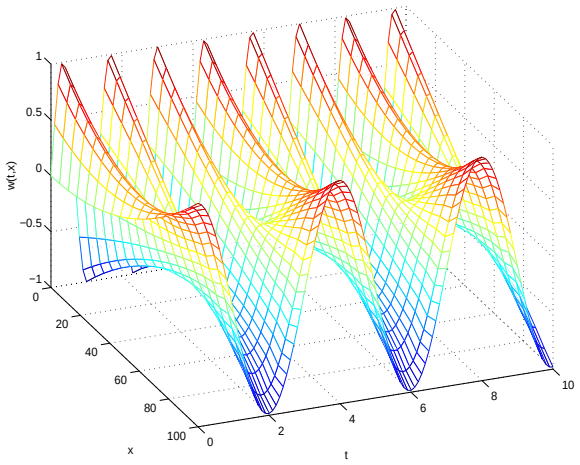

Figure 3.2: Numerical solution

shown on Figure 3.2. Observe that this is a problem with oscillating boundary conditions which can be manipulated by changing α and β. Also note that the exact solution and the numerical solution were plotted on the same scale, but with different angles of viewing. The absolute error at the final time was approximately .00823.

3.2 Burgers' Equation With Homogeneous Neumann Boundary Conditions

It is clear that from the Robin boundary conditions stated in the preceding section we can obtain the homomgeneous Neumann boundary conditions by setting $\kappa_1 = \kappa_2 = 0$. With that in mind, we will perform some examples with the two initial conditions $A\cos(.01\pi x)$ and $A(L/2 - x)^3$, where A is the magnitude of the initial condition function. Choosing $\epsilon = .94$, $\kappa = .55$, and $L = 100$, we compute the numerical solutions, generate 3-D plots of the solutions, and examine plots of the solutions at the initial time and the final time.

Example 3.2.1 In this example, we use $A(50-x)^3$ as the initial condition for our problem and compute the numerical solution with the appropriately chosen time length. Figure 3.3 is the numerical solution corresponding to $A = 1/12,500$ and the time length of 200,000

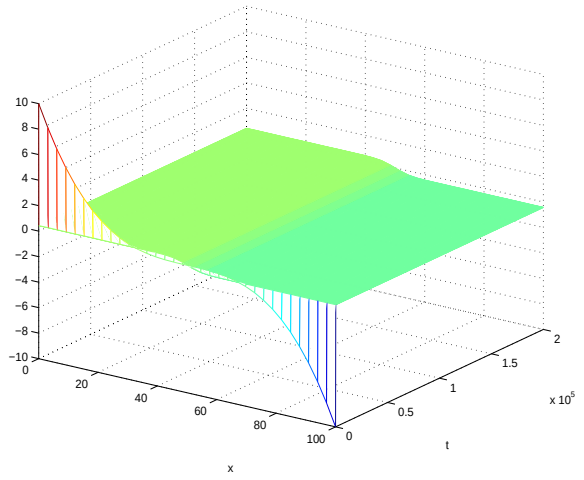

Figure 3.3: Numerical solution for $w_0(x) = \frac{(50-x)^3}{12{,}500}$

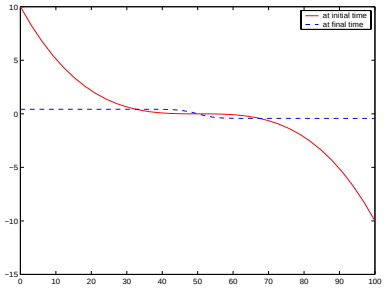

Figure 3.4: Initial and final time solutions

seconds. Figures 3.5, 3.7, and 3.9 are the numerical solutions corresponding to the values A of $-1/12,500$, $.4/50^3$ and $.1/50^3$, and with the time length of 500, 300,000, and 10,000 seconds respectively.

Example 3.2.2 Using $.4\cos(.01\pi x)$ and $-.4\cos(.01\pi x)$ as the initial conditions, we compute the numerical solutions with the time length of 200,000 and 2,500 seconds, respectively. Figures 3.11 and 3.12 are the numerical solutions for these two initial conditions.

In both examples, we notice that for *larger* initial conditions, the solution trajectories remain nonconstant throughout the whole chosen time length. However, for *small* initial data, the solution trajectories tend to converge to the zero constant solutions as shown in the plots of the solutions at the initial and final times. Therefore, for a fixed ϵ and for small initial data, numerical solutions to Burgers' equation with homogeneous Neumann boundary conditions tend to a constant function as t tends to infinity. Yet, for fixed ϵ and relatively large initial data, some numerical solutions converge to a nonconstant solution (cf [4], [1], [10], [15], [13]). But when we took the negative of the *larger* initial data, the trajectories converge to the zero solution.

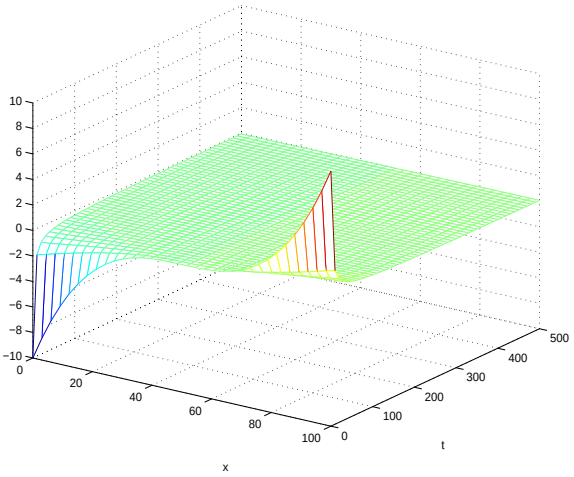

Figure 3.5: Numerical solution for $w_0(x) = -\frac{(50-x)^3}{12{,}500}$

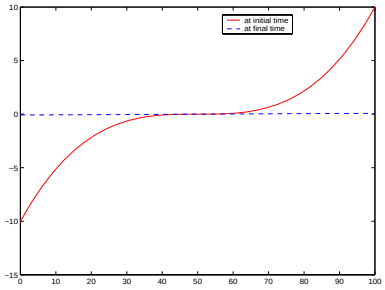

Figure 3.6: Initial and final time solutions

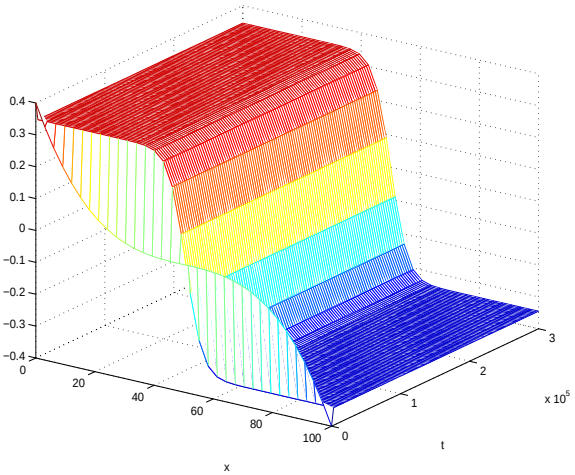

Figure 3.7: Numerical solution for $w_0(x) = \frac{.4(50-x)^3}{50^3}$

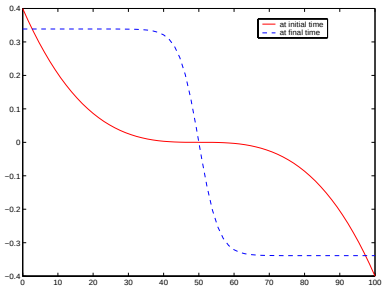

Figure 3.8: Initial and final time solutions

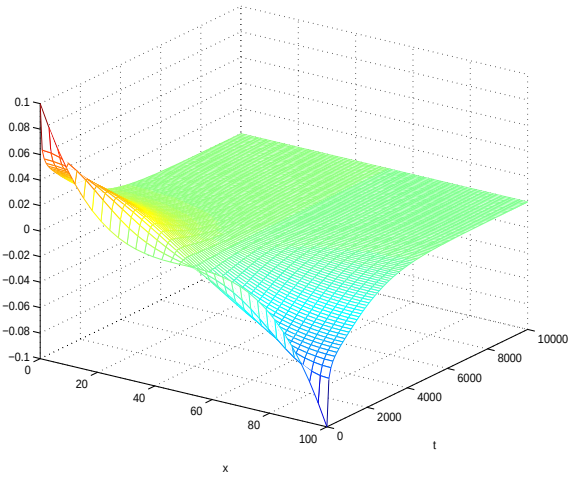

Figure 3.9: Numerical solution for $w_0(x) = \frac{.1(50-x)^3}{50^3}$

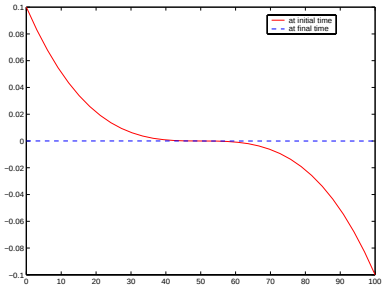

Figure 3.10: Initial and final time solutions

Upon examining the initial data used in these examples, we noticed they are functions that are odd about the midpoint of the interval $(0, L)$. Geometrically they are antisymmetric functions, which can be put in the class L_{AS} defined as follows

$$L_{AS} = \{\phi \in L^2(0, L) : \phi(x) = -\phi(L - x)\}. \tag{3.1}$$

These observations could be explained in the following manner. Consider the Burgers' equation with the homogeneous Neumann boundary conditions and the initial condition on the finite spatial domain

$$\frac{\partial w}{\partial t}(t, x) + w(t, x)\frac{\partial w}{\partial x}(t, x) = \epsilon \frac{\partial^2 w}{\partial x^2}(t, x) \tag{3.2}$$

$$\frac{\partial w}{\partial x}(t, 0) = 0 \tag{3.3}$$

$$\frac{\partial w}{\partial x}(t, L) = 0 \tag{3.4}$$

$$w(0, x) = \phi(x). \tag{3.5}$$

The corresponding steady state problem is

$$-\epsilon v_{xx}(x) + v(x)v_x(x) = 0 \tag{3.6}$$

$$v_x(0) = v_x(L) = 0. \tag{3.7}$$

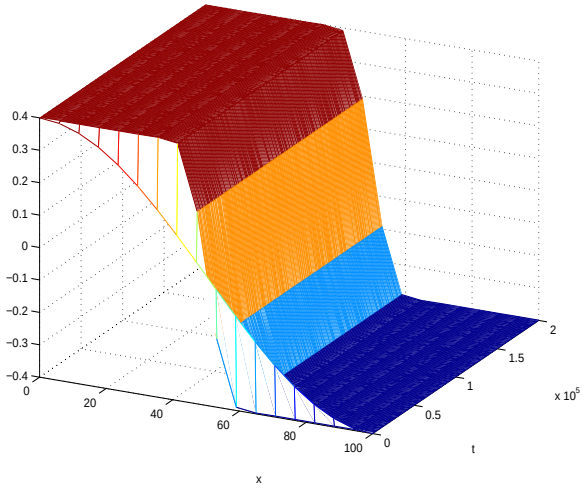

Figure 3.11: Numerical solution for $w_0(x) = .4\cos(.01\pi x)$

Equivalently we can rewrite the steady state equation (3.6) as

$$\left(-\epsilon v_x(x) + \frac{v^2(x)}{2}\right)_x = 0. \tag{3.8}$$

This equation implies that

$$-\epsilon v_x(x) + \frac{v^2(x)}{2} = c_0, \quad c_0 \in \Re. \tag{3.9}$$

Solving (3.9) yields

$$v(x) = \sqrt{2c_0}\tanh\left(\frac{\sqrt{2c_0}}{2\epsilon}(c-x)\right), \quad c_0, c \in \Re. \tag{3.10}$$

Differentiate this function $v(x)$ to get

$$v_x(x) = -\frac{c_0}{\epsilon}\operatorname{sech}^2\left(\frac{\sqrt{2c_0}}{2\epsilon}(c-x)\right), \tag{3.11}$$

Clearly the nonconstant function $v(x)$ in (3.10) satisfies (3.8), which in turn satisfies the steady state equation (3.6). However, the derivative function $v_x(x)$ does not vanish at $x = 0$ and $x = L$ except when c_0 is identically zero. Thus, the homogeneous Neumann boundary conditions could not be satisfied. This confirms the well-known fact that the only stationary solutions to Burgers' equation with homogeneous Neumann boundary conditions are constant solutions.

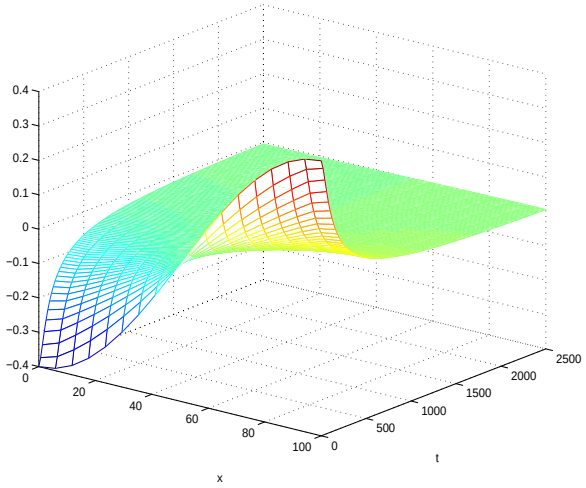

Figure 3.12: Numerical solution for $w_0(x) = -.4\cos(.01\pi x)$

At this point, it may seem that finding the nonconstant function $v(x)$ defined in (3.10) could be of no good advantage in dealing with the problem ((3.2) - (3.5)). However, if we are interested in studying Burgers' equation with the 'almost' homogeneous Neumann boundary conditions (e.g. $w_x(t,0) = -\gamma$ for some γ exponentially small positive number), then the nonconstant function $v(x)$ may perhaps be worth further examination.

3.3 Burgers' equation with nonhomogeneous Neumann boundary conditions

Before stating the problem for this section, we realize that in order for a function of the form given in (3.10) to be in the class $L_{AS}(0,L)$ defined in (3.1), the constant c in (3.10) must be chosen to be $L/2$. Hence we obtain functions $h(\cdot) \in L_{AS}(0,L)$ as follows

$$h(x) = \sqrt{2c_0}\tanh\left(\frac{\sqrt{2c_0}}{2\epsilon}(\frac{L}{2} - x)\right) \tag{3.12}$$

As we have noted, the function $h(x)$ given in (3.12) does satisfy the steady state equation (3.6) exactly but does not satisfy the boundary conditions (3.7). Still it can approximately satisfy the homogeneous boundary conditions to within exponentially small positive numbers

since

$$h'(0) = h'(L) = -\frac{c_0}{\epsilon}\text{sech}^2\left(\frac{L\sqrt{2c_0}}{4\epsilon}\right) = -\gamma, \tag{3.13}$$

where γ is chosen to be an exponentially small positive number. Thus for a small positive number γ, we can now replace the problem ((3.2) - (3.5)) by Burgers' equation with nonhomogeneous Neumann boundary conditions

$$\frac{\partial w}{\partial t}(t,x) + w(t,x)\frac{\partial w}{\partial x}(t,x) = \epsilon\frac{\partial^2 w}{\partial x^2}(t,x) \tag{3.14}$$

$$\frac{\partial w}{\partial x}(t,0) = -\gamma \tag{3.15}$$

$$\frac{\partial w}{\partial x}(t,L) = -\gamma \tag{3.16}$$

$$w(0,x) = \phi(x). \tag{3.17}$$

Then the associated stationary problem given below

$$-\epsilon v_{xx}(x) + v(x)v_x(x) = 0, \tag{3.18}$$

$$v_x(0) = v_x(L) = -\gamma, \tag{3.19}$$

will have solutions as the nonconstant functions $h(\cdot)$ given by (3.12). This naturally leads to the task of determining c_0 such that the condition $h'(0) = h'(L) = -\gamma$ holds. This means that we need to find c_0 that satisfies the equation

$$\frac{c_0}{\epsilon}\text{sech}^2\left(\frac{L\sqrt{2c_0}}{4\epsilon}\right) = \gamma. \tag{3.20}$$

With a little help from basic calculus, for fixed ϵ and γ, we find that there exist exactly two values c_{01} and c_{02} that solve (3.20). To varify this claim, let $s = \frac{L\sqrt{2c_0}}{4\epsilon}$, and rewrite the equation (3.20) in terms of s to get

$$\left(\frac{8\epsilon}{L}\right)s^2\text{sech}^2(s) = \gamma. \tag{3.21}$$

Now let the left-hand side of (3.21) be $g(s)$. Figure 3.13 is a typical graph of $g(s)$. From this graph we can see that in order for $h'(0) = h'(L) = -\gamma$, we have to pick those γ such that γ is less than the maximum value of g which occurs at the critical point $s \approx 1.2$ (See

γ	s_{01}	s_{02}	c_{01}	c_{02}
.25e-4	1.8548e-1	3.7038	2.4318e-5	9.6973e-3
.5e-4	2.6711e-1	3.2146	5.0434e-5	7.3046e-3
.7e-4	3.2095e-1	2.9642	7.2814e-5	6.2111e-3
1e-4	3.9322e-1	2.6849	1.0930e-4	5.0959e-3
1.5e-4	5.0472e-1	2.3402	1.8007e-4	3.8713e-3
3e-4	9.1496e-1	1.5380	5.9176e-4	1.6721e-3

Table 3.1: Numerically computed c_0

[1] and [4]). At this point, it is apparent that for fixed ϵ and γ, there are exactly two values c_{01} and c_{02} that solve equation (3.20). Hence there exist two types of nonconstant functions $h_{01}(\cdot)$ and $h_{02}(\cdot)$ corresponding to c_{01} and c_{02} respectively. Figure 3.14 is the graph of $h_{01}(x)$ for $\epsilon = .94$ and $c_0 = 7.2814e-5$, and Figure 3.15 is the plot of $h_{02}(x)$ for the same ϵ but for $c_0 = 6.2111e-3$. Table 3.1 is the table of values of c_{01} and c_{02} computed numerically with

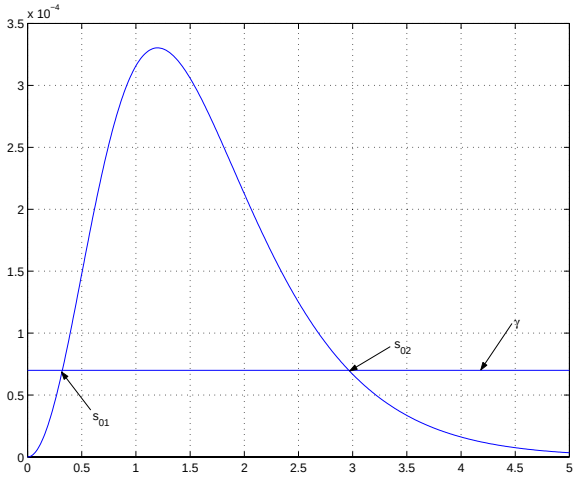

Figure 3.13: A typical graph of $g(s)$

$\epsilon = .94$ and $L = 100$. The parameter value γ is selected based on the graph of the function $g(s)$ in Figure 3.13. The s_{01} and s_{02} marked on Figure 3.13 are the solutions to (3.21) that will give the corresponding values c_{01} and c_{02} from $s = \frac{L\sqrt{2c_0}}{4\epsilon}$.

We will use some of these c_0 values for our examples presented in this section. We also will replace the non-homogeneous Neumann boundary conditions ((3.15) - (3.16)) for the

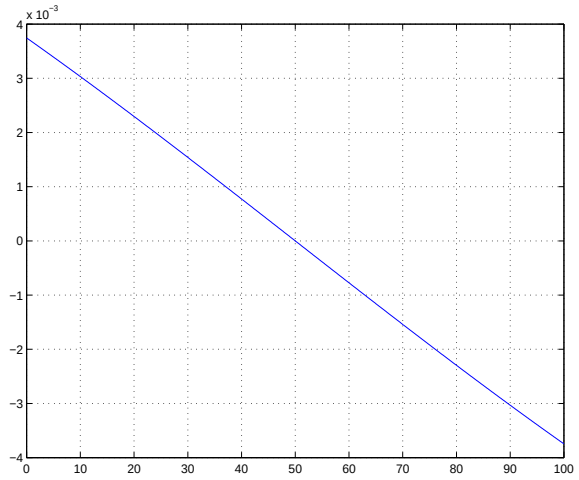

Figure 3.14: Graph of $h_{01}(\cdot)$

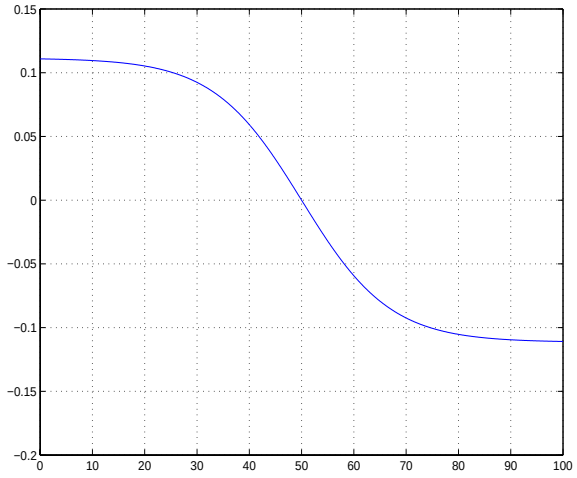

Figure 3.15: Graph of $h_{02}(\cdot)$

problem ((3.14) - (3.17)) by Burgers' equation with the boundary conditions

$$\frac{\partial w}{\partial t}(t,x) + w(t,x)\frac{\partial w}{\partial x}(t,x) = \epsilon \frac{\partial^2 w}{\partial x^2}(t,x) \tag{3.22}$$

$$-\kappa w_x(t,0) = \alpha_1 \tag{3.23}$$

$$\kappa w_x(t,L) = \alpha_2. \tag{3.24}$$

$$w(0,x) = w_0(x). \tag{3.25}$$

Note that in order to have the non-homogeneous Neumann boundary conditions as in (3.15) and (3.16), α_1 and α_2 must be chosen to be of opposite sign. This means that if $\alpha_1 > 0$ is assumed, then $\gamma = \frac{\alpha_1}{\kappa} = -\frac{\alpha_2}{\kappa}$.

Example 3.3.1 Choose $\kappa = .55$ and $\epsilon = .94$ with the initial condition $w_0(x) = .4\cos(.01\pi x)$. We computed and plotted the numerical solutions for the problem ((3.22) - (3.25)) corresponding to the values γ $2.5e-5, 7e-5$, and $3e-4$ from Table 3.1. As before, we also plotted the graph of the initial and final time solutions on the same axes. Figures 3.24, 3.20, and 3.16 correspond to the values γ being $.25e-4, .7e-4$, and $3e-4$ with the corresponding values c_{01} listed in Table 3.1. Figures 3.26, 3.22, and 3.18 correspond to the values γ being $.25e-4, .7e-4$, and $3e-4$ with the corresponding values c_{02} listed in Talble 3.1. We noticed that as we chose γ to be smaller and closer to 0, the numerical solution resembled the graph

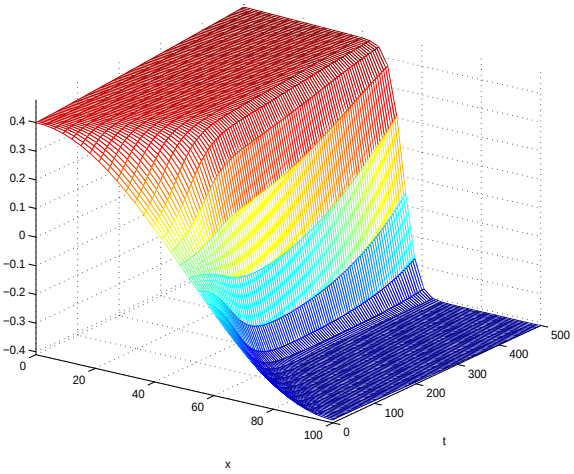

Figure 3.16: Numerical solution for $c_0 = 5.9176e-4$

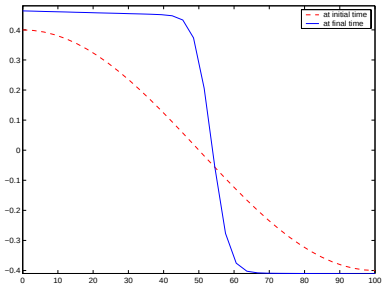

Figure 3.17: Initial and final time solutions

of the nonconstant function $h(\cdot)$ defined in (3.12).

Example 3.3.2 The parameters were chosen to be the same as in Example 3.3.1 but with the initial condition $.4(2/L)^3(L/2-x)^3$. However, in this example we only chose those c_0 values that corresponded to $\gamma = .25e-4$ (See Table 3.1). Figure 3.28 is the numerical solution for $c_0 = 2.4318e-5$, and Figure 3.30 corresponds to the value $c_0 = 9.6973e-3$. Both plots were generated with the final time being 500 seconds as in the previous examples.

3.4 Asymptotic Solutions

In this section, we examine the behavior of the numerical solutions to Burgers' equation as the nonhomogeneous Robin boundary conditions asymptotically approach the non-homogeneous Neumann boundary conditions. To see how this could be done numerically, recall that from

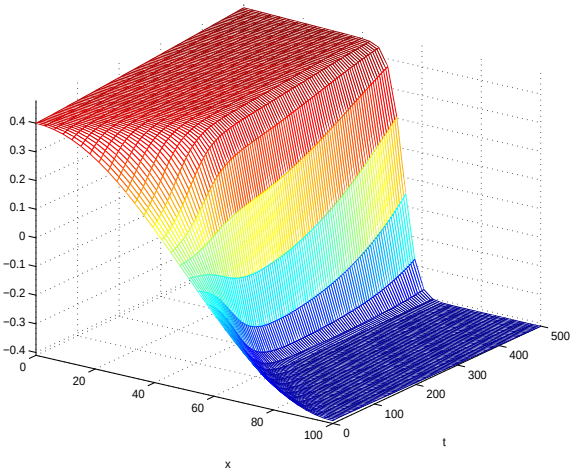

Figure 3.18: Numerical solution for $c_0 = 1.6721e - 3$

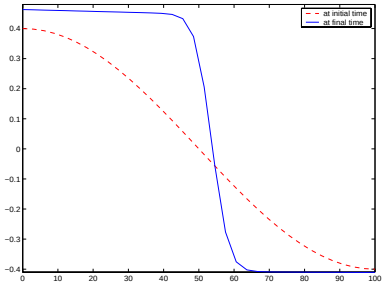

Figure 3.19: Initial and final time solutions

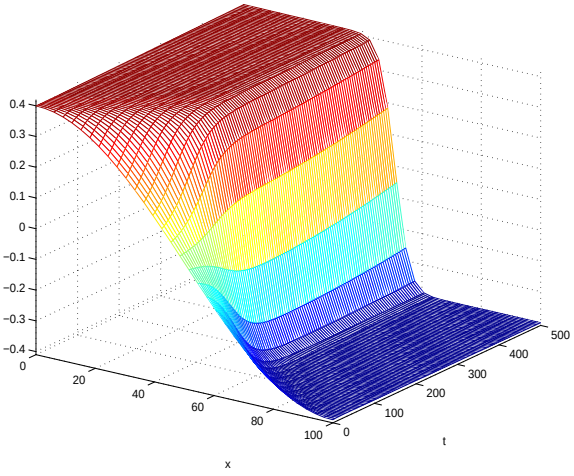

Figure 3.20: Numerical solution for $c_0 = 7.2814e - 5$

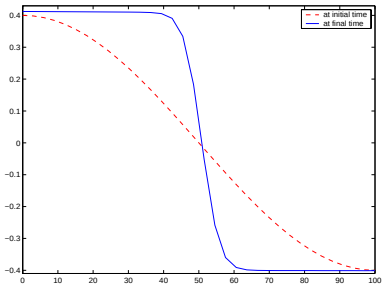

Figure 3.21: Initial and final time solutions

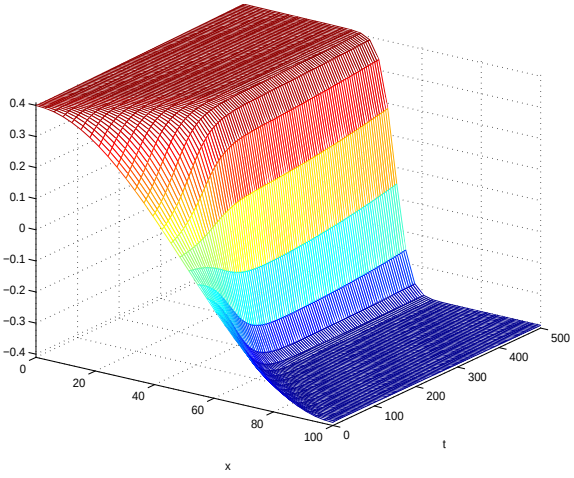

Figure 3.22: Numerical solution for $c_0 = 6.2111e - 3$

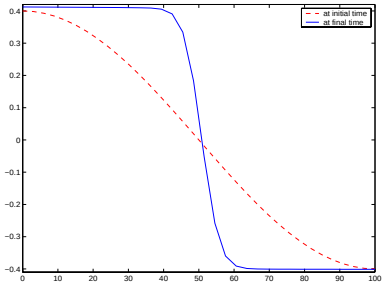

Figure 3.23: Initial and final time solutions

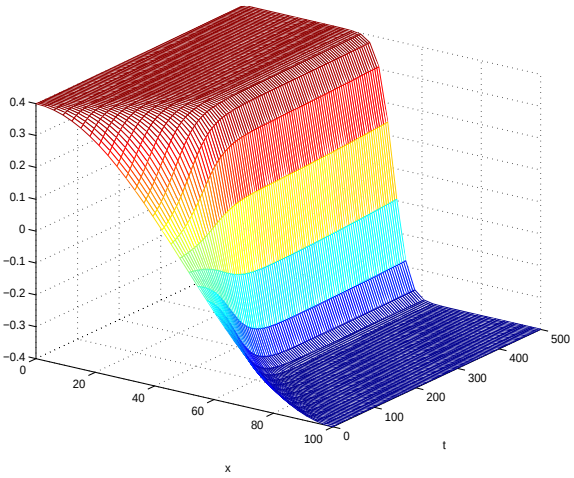

Figure 3.24: Numerical solution for $c_0 = 2.4318e - 5$

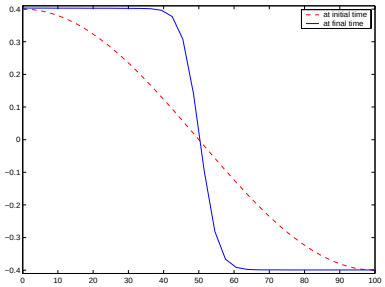

Figure 3.25: Initial and final time solutions

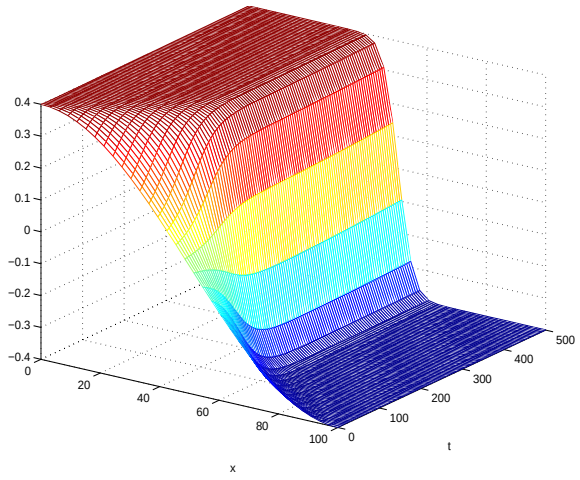

Figure 3.26: Numerical solution for $c_0 = 9.6973e - 3$

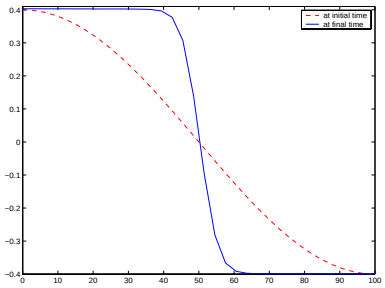

Figure 3.27: Initial and final time solutions

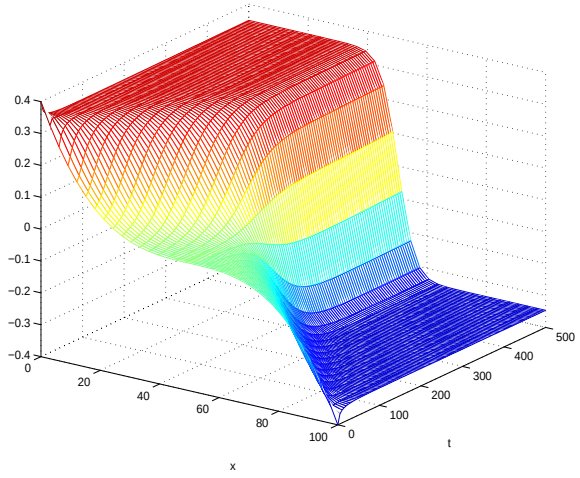

Figure 3.28: Numerical solution for $c_0 = 2.4318e - 5$

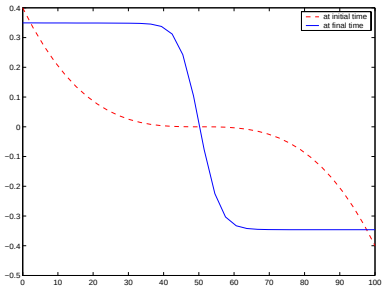

Figure 3.29: Initial and final time solutions

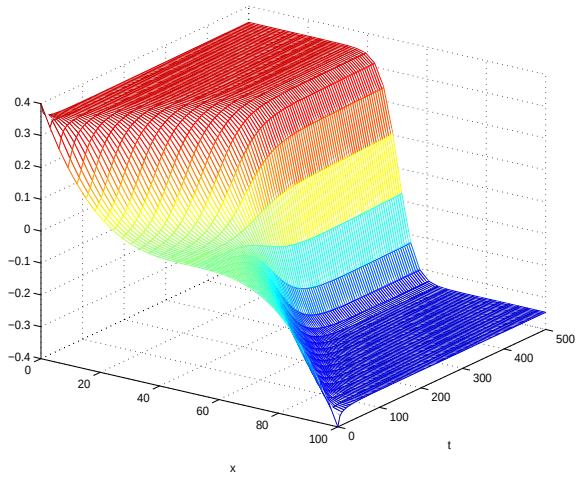

Figure 3.30: Numerical solution for $c_0 = 9.6973e - 3$

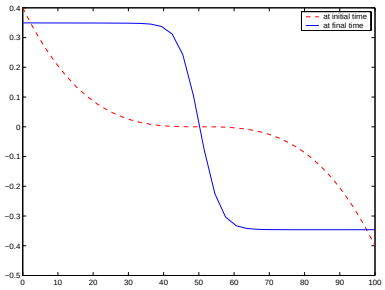

Figure 3.31: Initial and final time solutions

Section 1.5 in Chapter 1, the non-homogeneous Robin boundary conditions were of the form

$$\kappa_1 w(t,0) - \kappa \frac{\partial w}{\partial x}(t,0) = \alpha_1,$$
$$\kappa_2 w(t,L) + \kappa \frac{\partial w}{\partial x}(t,L) = \alpha_2,$$

with α_1 and α_2 given in ((1.42) - (1.43)). It is clear that in order for the non-homogeneous Robin boundary conditions to asymptotically approach the nonhomogeneous Neumann boundary conditions, κ_1 and κ_2 must approach zero. This can be achieved by diving κ_1 and κ_2 by some power of 2. Given the non-homogeneous Neumann boundary conditions in ((3.23) - (3.24)), the asymptotic solution is reached when the fractions $\frac{\alpha_1}{\kappa}$ and $\frac{\alpha_2}{\kappa}$ are close enough to the given parameter γ. In all examples presented here, we used the same parameters (e.g. ϵ, κ, etc.) as in the examples from the previous sections.

Example 3.4.1 We chose the initial condition to be $.4\cos(.01\pi x)$ and the c_0 values corresponding the value $\gamma = .25e - 4$. We generated the numerical solutions for $\kappa_1 = \kappa_2 = .124/2^{10}$ and for $\kappa_1 = \kappa_2 = .124/2^{15}$. Table 3.2 lists the numerical values of c_0, γ, α_1, α_2, $\frac{\alpha_1}{\kappa}$, $\kappa\gamma$ and $\kappa_1 h(0)$. Figures 3.32 and 3.34 are numerical solutions correponding to $c_0 = 2.4318e{-}5$ but with $\kappa 1 = \kappa 2 = .124/2^{10}$ and $\kappa 1 = \kappa 2 = .124/2^{15}$ respectively. Figures 3.36 and 3.38

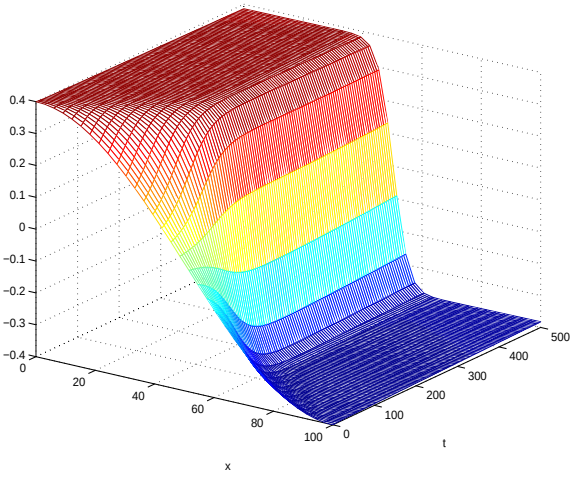

Figure 3.32: Numerical solution for $c_0 = 2.4318e-5$

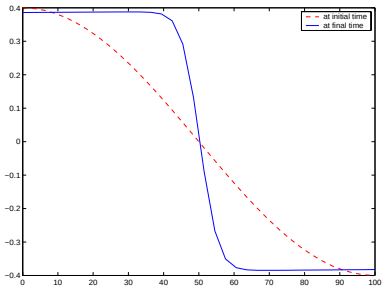

Figure 3.33: Initial and final time solutions

c_0	κ_1	$\alpha_1 = -\alpha_2$	γ	α_1/κ	$\kappa\gamma$	$\kappa_1 h(0)$
2.4318e-5	$.124/2^{10}$	1.3905e-5	.25e-4	.25283e-5	1.3750e-5	1.5486e-7
	$.124/2^{15}$	1.3755e-5	.25e-4	.25009e-5	1.3750e-5	4.8396e-9
9.6973e-3	$.124/2^{10}$	3.0594e-5	.25e-4	5.5625e-5	1.3750e-5	1.6844e-5
	$.124/2^{15}$	1.4276e-5	.25e-4	2.5957e-5	1.3750e-5	5.2636e-7

Table 3.2: Table of parameters numerically computed for Example 3.4.1

correspond to the same κ_1 and κ_2 but with $c_0 = 9.6973e-3$. Note for those smaller values of κ_1 and κ_2, the plots approximately yield the non-homogeneous Neumann results.

Example 3.4.2 With the same parameters c_0 and γ as in the preceding example, we chose the initial condition to be $.4(2/L)^3(L/2-x)^3$. As in Example 3.4.1, we computed the numerical solutions for $\kappa_1 = \kappa_2 = .124/2^{10}$ and for $\kappa_1 = \kappa_2 = .124/2^{15}$ and plotted the solutions. Table 3.3 lists the numerical values of c_0, γ, α_1, α_2, $\frac{\alpha_1}{\kappa}$, $\kappa\gamma$ and $\kappa_1 h(0)$. Figures 3.40 and 3.42 are numerical solutions correponding to $c_0 = 2.4318e-5$ but with $\kappa 1 = \kappa 2 = .124/2^{10}$ and $\kappa 1 = \kappa 2 = .124/2^{15}$ respectively. Figures 3.44 and 3.46 correspond to the same κ_1 and κ_2 but with $c_0 = 9.6973e-3$. Note for those smaller values of κ_1 and κ_2, the plots approximately yield the non-homogeneous Neumann results. The initial and final solutions were also plotted on the same the axes.

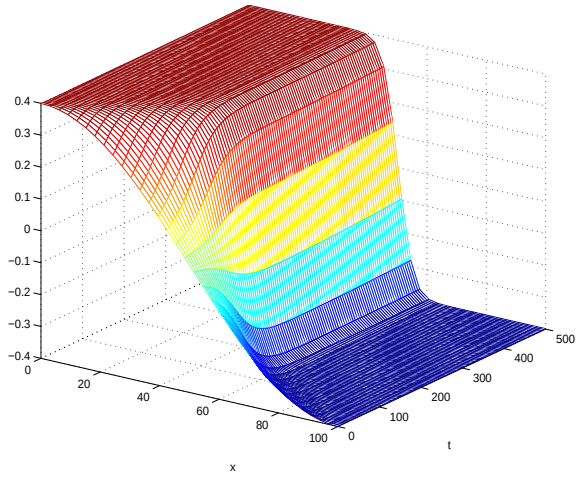

Figure 3.34: Numerical solution for $c_0 = 2.4318e-5$

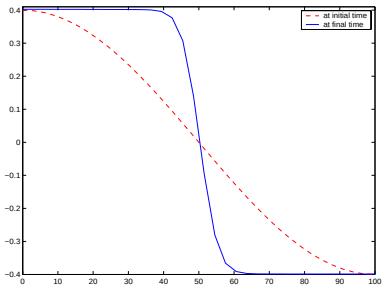

Figure 3.35: Initial and final time solutions

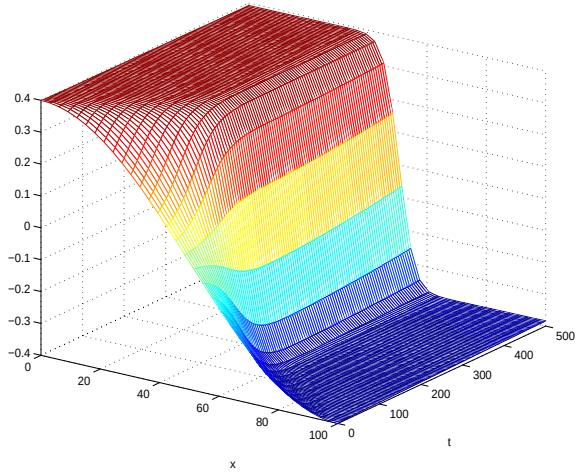

Figure 3.36: Numerical solution for $c_0 = 9.6973e-3$

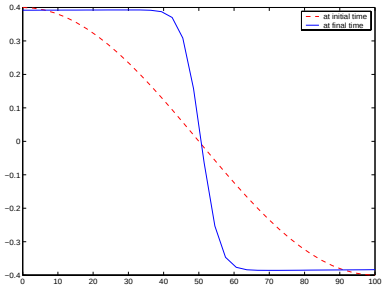

Figure 3.37: Initial and final time solutions

c_0	κ_1	$\alpha_1 = -\alpha_2$	γ	α_1/κ	$\kappa\gamma$	$\kappa_1 h(0)$
2.4318e-5	$.124/2^{10}$	1.3905e-5	.25e-4	.25282e-5	1.3750e-5	1.5486e-7
	$.124/2^{15}$	1.3755e-5	.25e-4	.25009e-5	1.3750e-5	4.8395e-9
9.6973e-3	$.124/2^{10}$	3.0594e-5	.25e-4	5.5625e-5	1.3750e-5	1.6844e-5
	$.124/2^{15}$	1.4276e-5	.25e-4	2.5957e-5	1.3750e-5	5.2636e-7

Table 3.3: Table of parameters numerically computed for Example 3.4.2

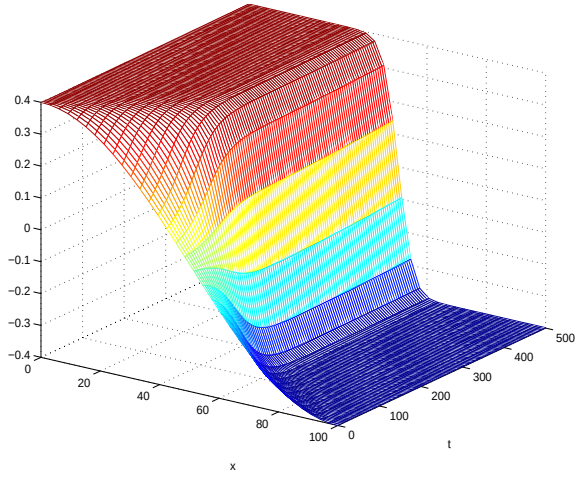

Figure 3.38: Numerical solution for $c_0 = 9.6973e - 3$

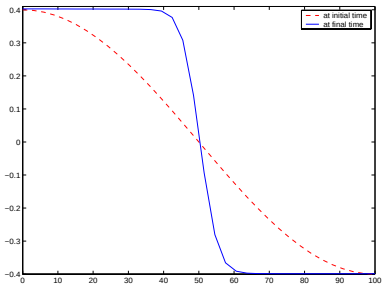

Figure 3.39: Initial and final time solutions

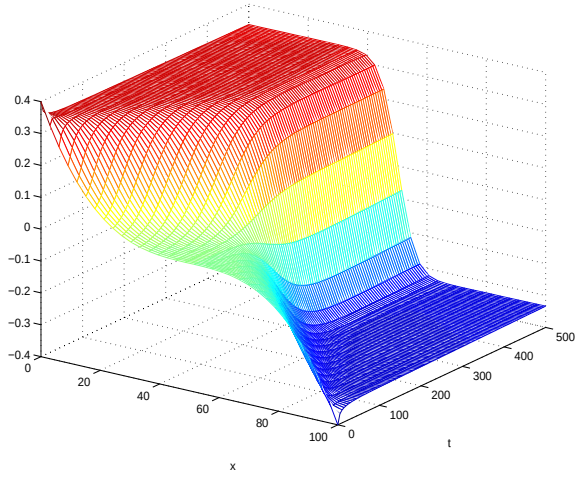

Figure 3.40: Numerical solution for $c_0 = 2.4318e - 5$

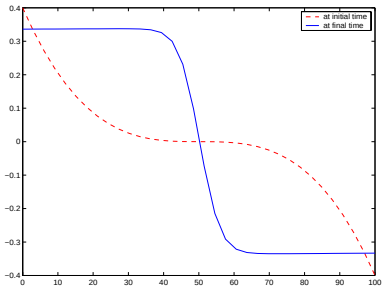

Figure 3.41: Initial and final time solutions

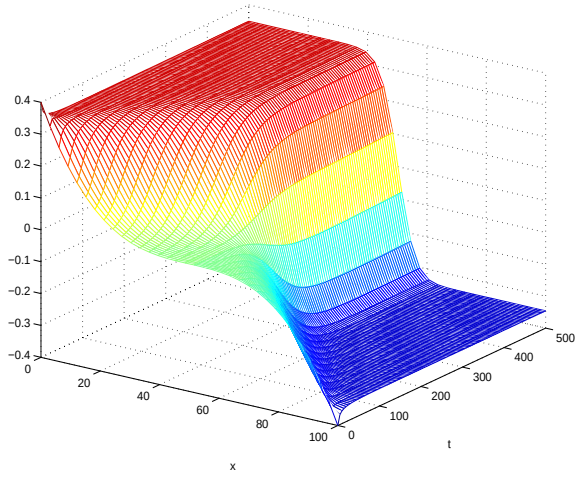

Figure 3.42: Numerical solution for $c_0 = 2.4318e - 5$

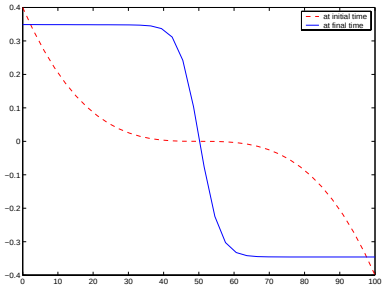

Figure 3.43: Initial and final time solutions

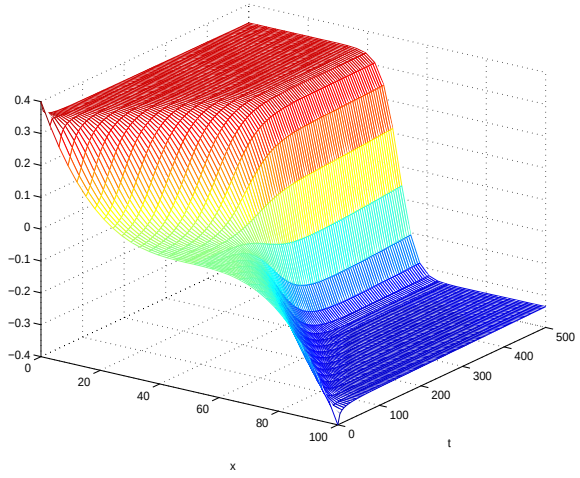

Figure 3.44: Numerical solution for $c_0 = 9.6973e - 3$

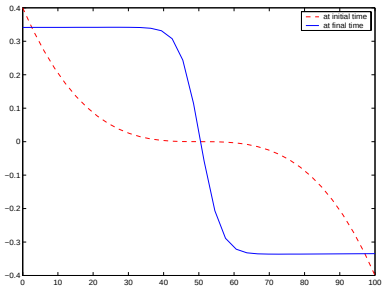

Figure 3.45: Initial and final time solutions

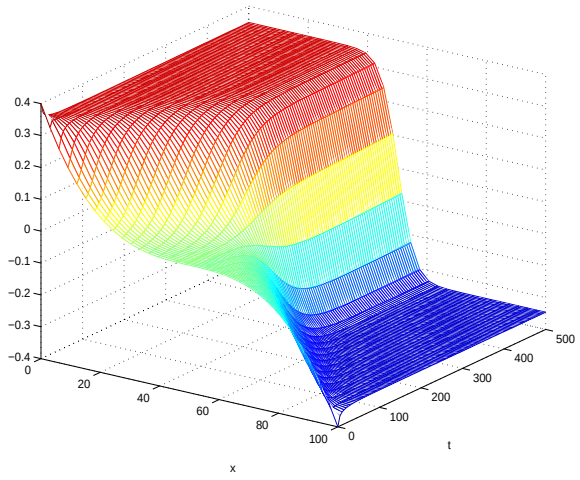

Figure 3.46: Numerical solution for $c_0 = 9.6973e-3$

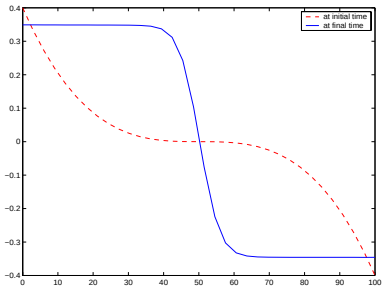

Figure 3.47: Initial and final time solutions

Example 3.4.3 In this example, we replaced the initial condition in Example 3.4.1 and Example 3.4.2 by $w_0(x) = 12.8(L/4-x)(L/2-x)(3L/4-x)/(3L^3)$ with $L = 100$. We again used the same c_0 corresponding to $\gamma = .25e-4$, and other parameters were the same as in all the preceding examples. We first computed and plotted the numerical solutions for the non-homogeneous Neumann cases. Figures 3.48 and 3.50 are the plots of the numerical solutions in this case for $c_0 = 2.4318e-5$ and $c_0 = 9.6973e-3$, respectively. We then computed and plotted the numerical solutions for the problem where we let the non-homogeneous Robin boundary conditions asymptotically approach the non-homogeneous Neumann boundary conditions. Based on the results from the two preceding examples in this section, we computed the asymptotic solutions only for $\kappa_1 = \kappa_2 = .124/2^{15}$. Figures 3.52 and 3.54 are the numerical solutions in this case with c_0 being $2.4318e-5$, and $9.6973e-3$.

3.5 Burgers' equation with nonhomogeneous Robin boundary conditions

Finally, we conclude Chapter 3 by examining the behavior of the numerical solutions to Burgers' equation with the non-homogeneous Robin boundary conditions as stated in Section

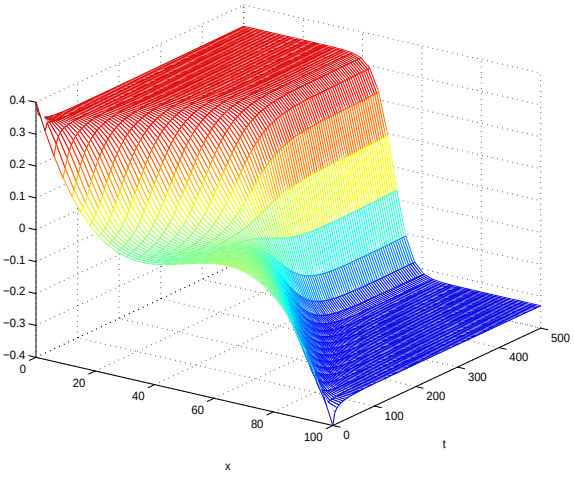

Figure 3.48: Numerical solution for $c_0 = 2.4318e - 5$

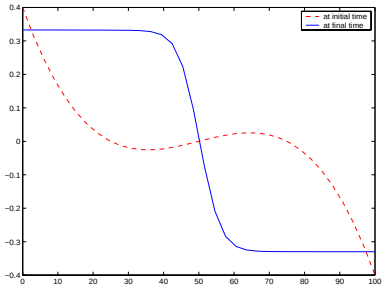

Figure 3.49: Initial and final time solutions

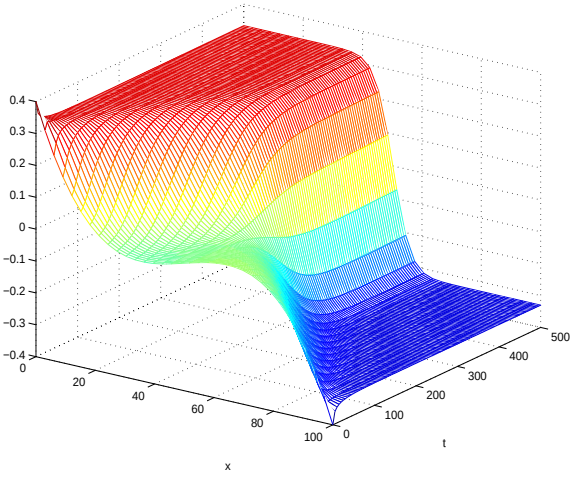

Figure 3.50: Numerical solution for $c_0 = 9.6973e - 3$

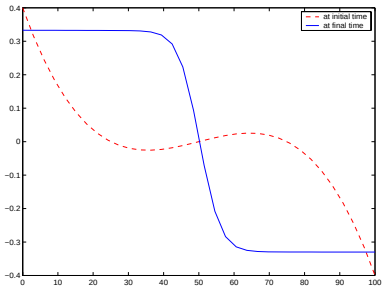

Figure 3.51: Initial and final time solutions

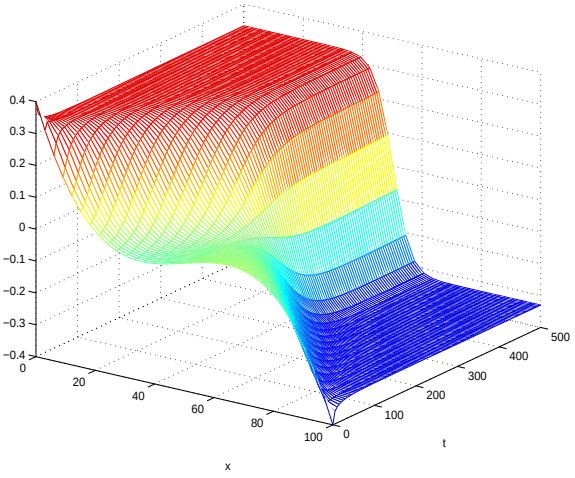

Figure 3.52: Numerical solution for $c_0 = 2.4318e-5$ where Robin approaches Neumann conditions

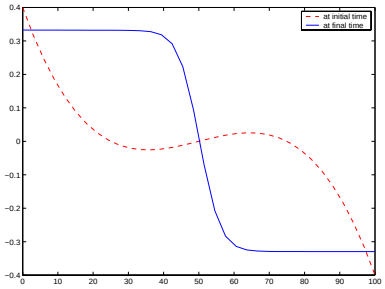

Figure 3.53: Initial and final time solutions

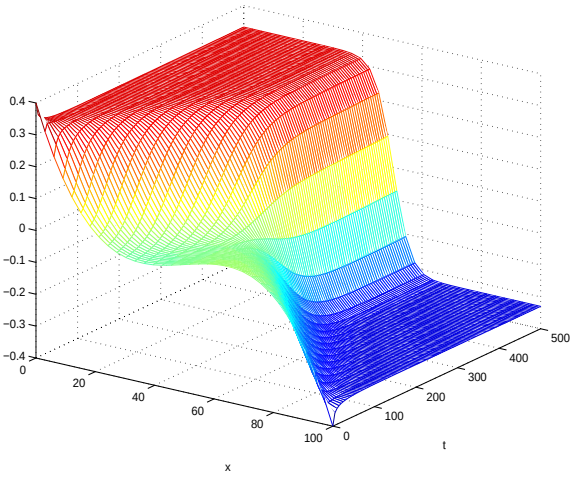

Figure 3.54: Numerical solution for $c_0 = 9.6973e-3$ where Robin approaches Neumann conditions

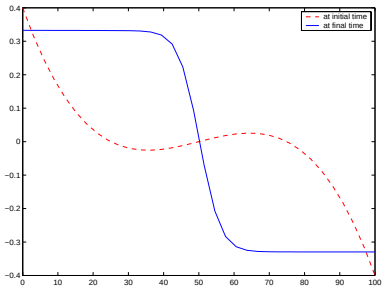

Figure 3.55: Initial and final time solutions

1.5 of Chapter 1, which we restate here

$$\frac{\partial w}{\partial t}(t,x) + w(t,x)\frac{\partial w}{\partial x}(t,x) = \epsilon\frac{\partial^2 w}{\partial x^2}(t,x), \qquad 0 < x < L, \qquad t > 0, \tag{3.27}$$
$$\kappa_1 w(t,0) - \kappa\frac{\partial w}{\partial x}(t,0) = \alpha_1,$$
$$\kappa_2 w(t,L) + \kappa\frac{\partial w}{\partial x}(t,L) = \alpha_2,$$
$$w(0,x) = w_o(x).$$

Both α_1 and α_2 are to be computed by the following

$$\alpha_1 = \kappa_1 h(0) - \kappa h'(0), \tag{3.28}$$
$$\alpha_2 = \kappa_2 h(L) + \kappa h'(L). \tag{3.29}$$

Again, in all the examples represented here, we chose $\epsilon = .94$, $\kappa_1 = \kappa_2 = .124$, and $\kappa = .55$. Because the nonconstant function $h(\cdot)$ is antisymmetric on $[0, L]$, $h(0) = -h(L)$; and since $h'(0) = h'(L) = -\gamma$, we noted that $\alpha_1 = -\alpha_2$, where they are defined in (3.28). As for the initial conditions, we used the three different conditions that were used in the preceding examples.

Example 3.5.1 The initial condition for this example is again $.4\cos(.01\pi x)$. The numerical solutions were computed for c_0 values corresponding to $\gamma = .25e - 4$. As before we plotted the numerical solutions for those c_0 values. Figures 3.56 and 3.58 are the numerical solutions for smaller and larger c_0.

Example 3.5.2 The initial conditions used here are $.4(2/L)^3(L/2 - x)^3$ and $12.8(L/4 - x)(L/2 - x)(3L/4 - x)/(3L^3)$. For the former initial condition, Figures 3.60 and 3.62 are the numerical solutions for smaller and larger c_0; and for the later condition, Figures 3.64 and 3.66 are the numerical solutions for smaller and larger c_0.

Based on the graphs of the initial and final time solutions for all three initial conditions, we noticed that the solutions at the final times did not quite represent the general shape of the nonconstant functions $h(\cdot)$ discussed in Section 3.3 of this chapter. However, these

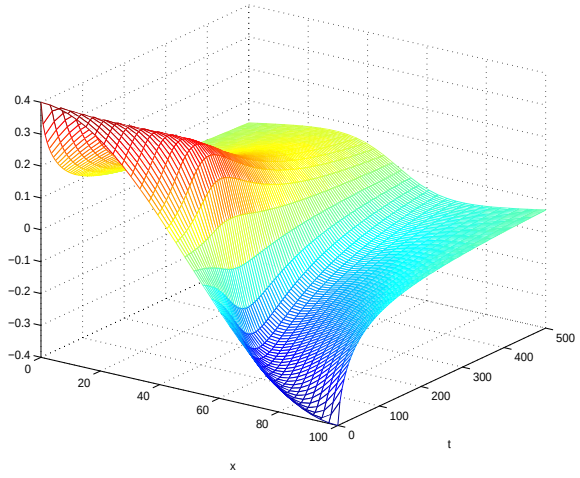

Figure 3.56: Numerical solution for $c_0 = 2.4318e - 5$

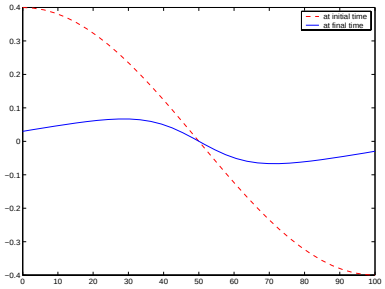

Figure 3.57: Initial and final time solutions

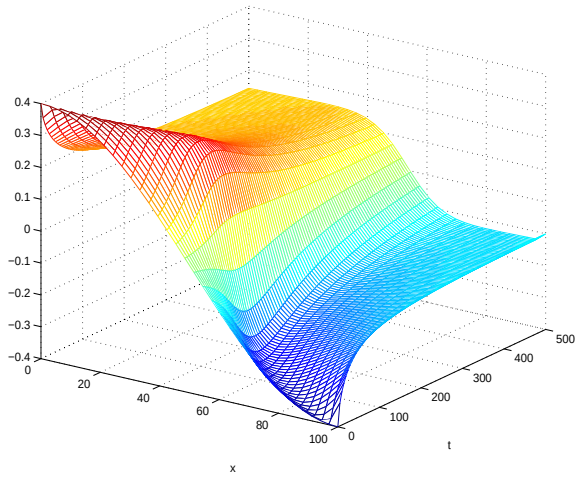

Figure 3.58: Numerical solution for $c_0 = 9.6973e - 3$

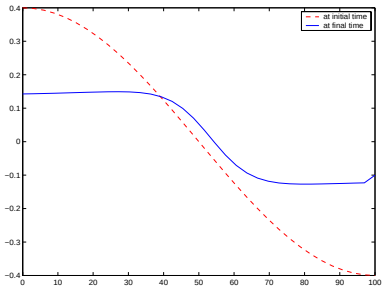

Figure 3.59: Initial and final time solutions

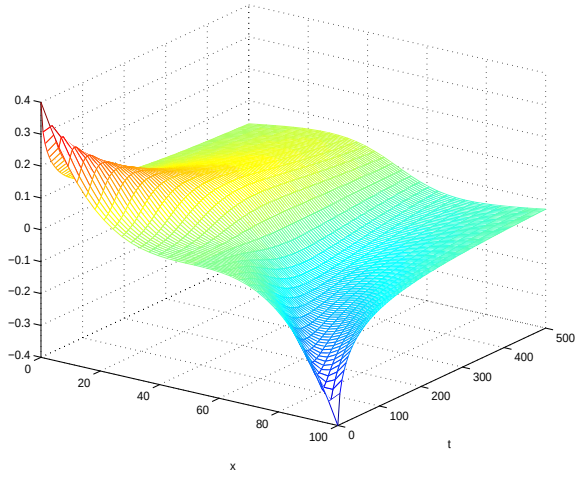

Figure 3.60: Numerical solution for $c_0 = 2.4318e - 5$

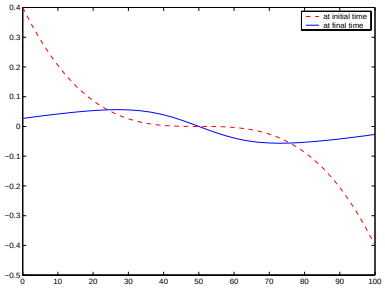

Figure 3.61: Initial and final time solutions

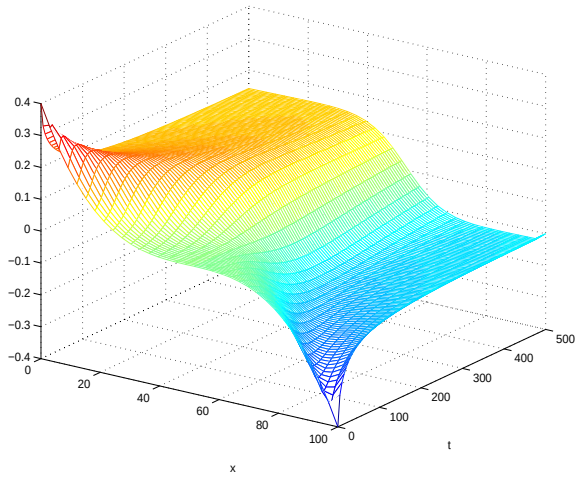

Figure 3.62: Numerical solution for $c_0 = 9.6973e - 3$

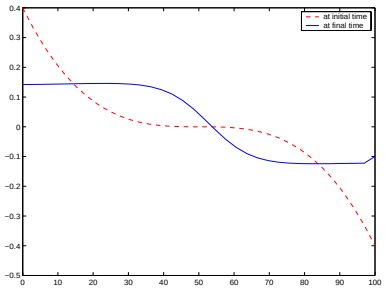

Figure 3.63: Initial and final time solutions

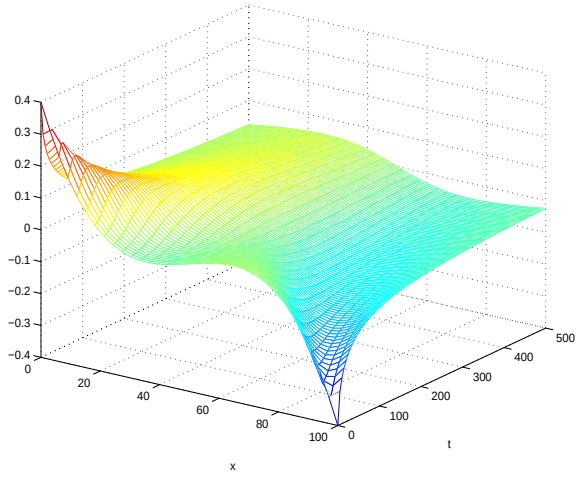

Figure 3.64: Numerical solution for $c_0 = 2.4318e - 5$

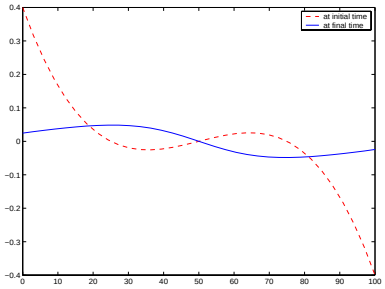

Figure 3.65: Initial and final time solutions

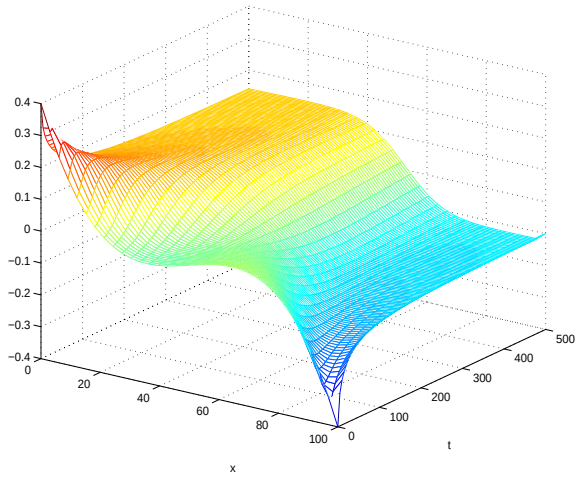

Figure 3.66: Numerical solution for $c_0 = 9.6973e - 3$

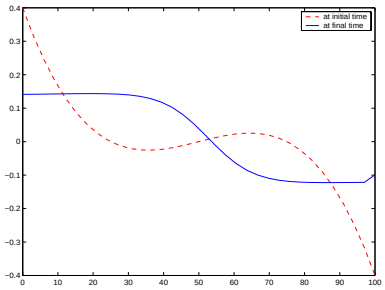

Figure 3.67: Initial and final time solutions

plots do have characteristics similar to those functions $h(\cdot)$. They are all antisymmetric on the spatial domain except for those in Figures 3.59, 3.63 and 3.67. This may be explained by the numerical errors that were accumulated from the ODE23S Solver and the Galerkin/Conservation finite element method.

The next issue that we would like to explore numerically is whether or not the steady state solutions to the problem with the non-homogeneous Robin condition and the steady state solutions the problem with the homogeneous Robin condition are constant and identical. Because of the type of initial conditions that we choose here, the constant steady state solution to both problems should be the zero steady state solution.

Example 3.5.3 Using the same initial conditions as in the two preceding examples, we numerically approximate the problem with the homogeneous Robin boundary conditions. We use the smaller c_0 value corresponding to $\alpha = .25e - 4$ in this example. The final time for the simulation is 1,500 seconds. Each figure has the plot for the numerical solution in 3-D and the graphs of the solutions at the initial time and final time. Figure 3.68 is the numerical solution for the problem with $12.8(L/4 - x)(L/2 - x)(3L/4 - x)/(3L^3)$, where $L = 100$. Figures 3.69 and 3.70 are the numerical solutions corresponding to the initial conditions $.4\cos(.01\pi x)$ and $.4(2/L)^3(L/2 - x)^3$, respectively.

As expected, zero is the steady state solution for the homogeneous Robin condition. We would expect the difference between the homogeneous and non-homogeneous cases to be that the steady state solution for the non-homogeneous case converges to zero slower than the homogeneous case. Figure 3.71 shows the numerical steady state solution for the non-homogeneous case with the initial condition $12.8(L/4 - x)(L/2 - x)(3L/4 - x)/(3L^3)$. And the final time for this example is 2,000 seconds. Even with longer time length, the plot of the solution at the final time is not quite the zero solution. This confirms that the non-homogeneous Robin problem converges to the zero steady state solution slower than the homogeneous problem.

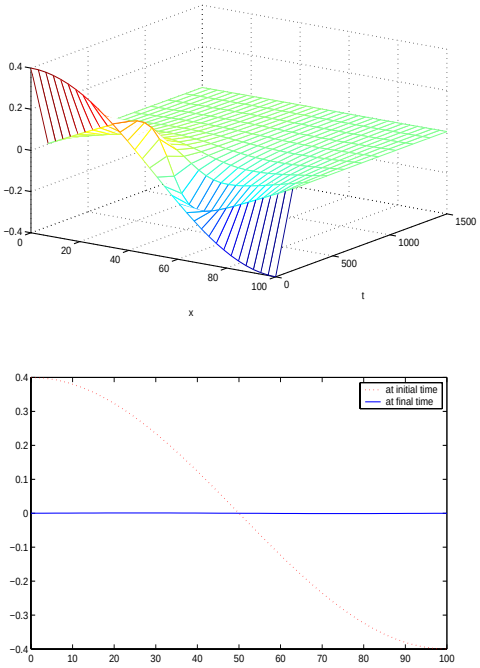

Figure 3.68: Numerical solution for the homogeneous Robin case

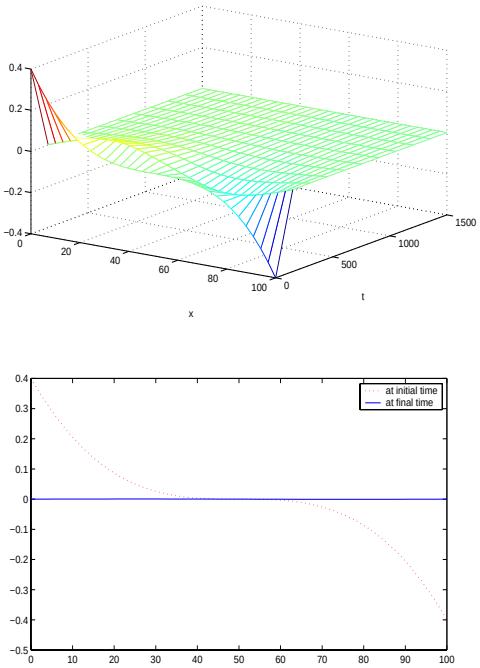

Figure 3.69: Numerical solution for the homogeneous Robin case

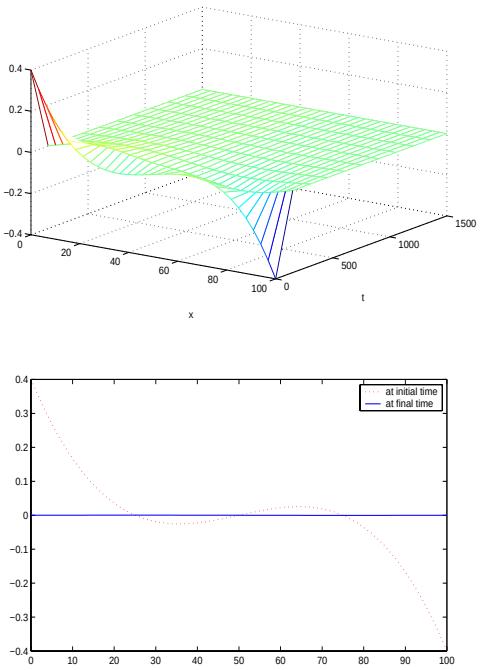

Figure 3.70: Numerical solution for the homogeneous Robin case

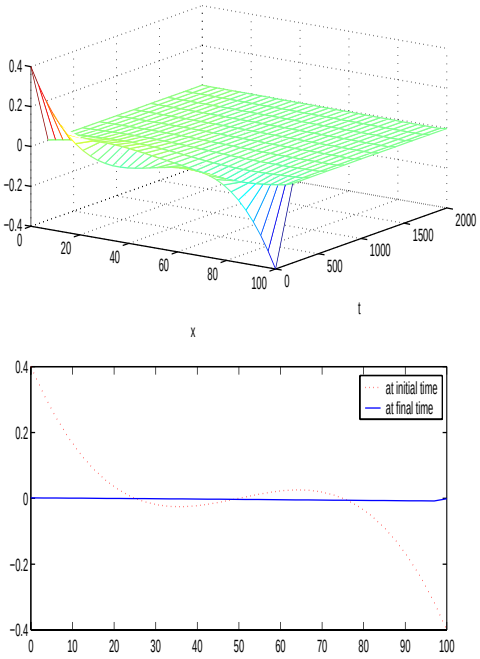

Figure 3.71: Numerical solution for the non-homogeneous Robin case

Chapter 4

Conclusions

4.1 Summary

In this thesis, we used the finite element method to numerically solve the initial boundary value problem

$$\begin{aligned}
\frac{\partial w}{\partial t}(t,x) + w(t,x)\frac{\partial w}{\partial x}(t,x) &= \epsilon\frac{\partial^2 w}{\partial x^2}(t,x) + f(t,x), \qquad 0 < x < L, \qquad t > 0, \qquad (4.1)\\
\kappa_1 w(t,0) - \kappa\frac{\partial w}{\partial x}(t,0) &= \alpha_1, ,\\
\kappa_2 w(t,L) + \kappa\frac{\partial w}{\partial x}(t,L) &= \alpha_2, ,\\
w(0,x) &= w_o(x), .
\end{aligned}$$

where α_1 and α_2 were given by

$$\alpha_1 = \kappa_1 h(0) - \kappa h'(0), \qquad (4.2)$$

$$\alpha_2 = \kappa_2 h(L) + \kappa h'(L), \qquad (4.3)$$

with $h(x)$ being antisymmetric at $x = L/2$ on the interval $(0, L)$

$$h(x) = \sqrt{2c_0}\ tanh\left(\frac{\sqrt{2c_0}}{2\epsilon}(L/2 - x)\right). \qquad (4.4)$$

We first numerically solved the initial boundary value problem for the non-homogeneous Burgers' equation on a finite domain with a known solution to test the accuracy of our

scheme. Then we numerically approximated the homogeneous Burgers' equation with the homogeneous Neumann boundary condition on a finite domain $(0, L)$ with different initial conditions. The numerical results for the Neumann problem were the same as those found in [1], [4], [13] and [15].

When we investigated the problem in which the non-homogeneous Robin boundary conditions asymptotically approach the non-homogeneous Neumann boundary conditions, we noticed that if the value α_1/κ is near γ, the numerical solutions approximate the non-homogeneous Neumann results. We also studied the behavior of the numerical solutions to Burgers' equation with the non-homogeneous Robin boundary conditions. Using the smallest γ value listed in Table 3.1, we numerically approximated this problem with three different initial conditions in the class of antisymmetry L_{AS}. We found that, for the smaller value c_0 corresponding to the chosen γ, the numerical solutions at the final time appeared to belong to L_{AS}. Yet, for the bigger value c_0, the numerical solutions at the final time did not belong to L_{AS}. Perhaps, this could be the numerical error arising from the ODE23S Solver and the finite element scheme that we used.

4.2 Conclusion

In this thesis, we confirmed the numerical solutions observed by other researchers for the Neumann boundary conditions (See [1], [4], [13] and [15]). We also showed that the non-homogeneous Robin boundary problem has non-constant steady state solutions similar to the Neumann problem. Moreover, these solutions solve a nearby homogeneous Robin problem. As we examined the case in which the Robin boundary conditions approach the Neumann boundary conditions, we observed that the numerical solutions approach the solutions corresponding to the Neumann boundary problem. Thus, numerical problems occur as in the Neumann case. Note also that all these results depend on how close the problem is to a Neumann problem and on the *shape* and *size* of the initial data. However, the exact

nature of this dependence remains unknown both theoretically and numerically.

4.3 Open Problems

Although the work in this thesis is purely numerical, it is our hope that the numerical results here give rise to sereval interesting questions. Perhaps, one could consider the following problems:

- Can one find more theoretical results similar to those found in [1]?
- Can there be another class of initial data that might give rise to numerical anomaly as the class of initial data in L_{AS} does?
- Is it possible to construct a numerical scheme that overcomes the problems with current schemes?

Bibliography

[1] E. Allen, J. Burns, D. Gilliam, J. Hill, and V. Shubov. The impact of finite precision arithmetic and sensitivity on the numerical solution of partial differential equations. *Journal of Computational Physics*, 1999.

[2] H. Bateman. Some recent researches on the motion of fluids. *Mon. Weather Rev.*, 43:163–170, 1915.

[3] J. M. Burgers. A mathematical model illustrating the theory of turbulence. *Adv. in App. Mech.*, 1:171–199, 1948.

[4] J. Burns, A. Balogh, D. S. Gilliam, and V. I. Shubov. Numerical stationary solutions for a viscous burgers' equation. *Journal of Mathematical Systems, Estimation, and Control*, 8:1–16, 1998.

[5] J. D. Cole. On a quasi-linear parabolic equation occurring in aerodynamics. *Quart. Appl. Math*, 9:225–236, 1951.

[6] Clive A. J. Fletcher. Burgers' equation: A model for all reasons. In J. Noye, editor, *Numerical Solutions of Partial Differential Equations*, pages 139–225. North-Holland Publishing Company, 1982.

[7] E. Hopf. The partial differential equation $u_t + uu_x = \mu u_{xx}$. *Comm. Pure & Applied Math*, 3:201–230, 1950.

[8] G. Kreiss and H. Kreiss. Convergence to steady state of solutions of burgers' equation. *Applied Numerical Mathematics*, 2:161–179, 1986.

[9] M. J. Lighthill. Viscosity effects in sound waves of finite amplitude. In G. K. Batchelor and R. M. Davies, editors, *Surveys in Mechanics*, pages 250–351. C.U.P., Cambridge, 1956.

[10] H. Marrekchi. *Dynamic Compensators for a Nonlinear Conservation Law.* PhD thesis, Virginia Tech, Blacksburg, VA, 1993.

[11] Kenneth L. Massa. Burgers' equation. Master's thesis, Virginia Tech, Blacksburg, VA, 1997.

[12] J. P. Moran and S. F. Shen. On the formation of weak plane shock waves by impulsive motion of a piston. *Journal of Fluid Mechanics*, 25:705–718, 1966.

[13] Steven M. Pugh. Finite element approximations of Burgers' equation. Master's thesis, Virginia Tech, Blacksburg, VA, 1995.

[14] L. G. Reyna and M. J. Ward. On the exponentially slow motion of a viscous shock. *Comm. Pure Appl. Mathematics*, XLVIII:79–120, 1995.

[15] Lyle C. Smith. Finite element approximation of Burgers' equation with Robin boundary conditions. Master's thesis, Virginia Tech, Blacksburg, VA, 1997.

Vita

Vinh Quoc Nguyen was born in Saigon, Vietnam on January 6, 1969. He attended Virginia Polytechnic Institute and State University in 1996 and received Bachelor of Science in Applied Computational Mathematics in 1998. He continued his education at Virginia Tech and received Master of Science in Applied Computational Mathematics in 2001. He is a member of Pi Mu Epsilon National Mathematics Honorary Society. He begins to work in June 2001 as a summer intern at the Applied Physics Laboratory at Johns Hopkins University in Columbia, Maryland.